

# We are IntechOpen, the world's leading publisher of Open Access books Built by scientists, for scientists

6,300

Open access books available

171,000

International authors and editors

190M

Downloads

Our authors are among the

154

Countries delivered to

TOP 1%

most cited scientists

12.2%

Contributors from top 500 universities



WEB OF SCIENCE™

Selection of our books indexed in the Book Citation Index  
in Web of Science™ Core Collection (BKCI)

Interested in publishing with us?  
Contact [book.department@intechopen.com](mailto:book.department@intechopen.com)

Numbers displayed above are based on latest data collected.  
For more information visit [www.intechopen.com](http://www.intechopen.com)



## Chapter

# Fluorescent Markers: Proteins and Nanocrystals

*Anielle Christine Almeida Silva, Jerusa Maria de Oliveira, Kelen Talita Romão da Silva, Francisco Rubens Alves dos Santos, João Paulo Santos de Carvalho, Rose Kethelyn Souza Avelino, Eurípedes Alves da Silva Filho, Marcelo Duzzioni, Edigar Henrique Vaz Dias, Fábio de Oliveira, Juliana Rodrigues Machado, Malu Mateus Santos, Marcos Vinícius da Silva, Carlo José Freire de Oliveira, Virmondes Rodrigues Junior, Lucas Anhezini and Noelio Oliveira Dantas*

## Abstract

This book chapter will comment on fluorescent reporter proteins and nanocrystals' applicability as fluorescent markers. Fluorescent reporter proteins in the *Drosophila* model system offer a degree of specificity that allows monitoring cellular and biochemical phenomena *in vivo*, such as autophagy, mitophagy, and changes in the redox state of cells. Titanium dioxide (TiO<sub>2</sub>) nanocrystals (NCs) have several biological applications and emit in the ultraviolet, with doping of europium ions can be visualized in the red luminescence. Therefore, it is possible to monitor nanocrystals in biological systems using different emission channels. CdSe/CdS magic-sized quantum dots (MSQDs) show high luminescence stability in biological systems and can be bioconjugated with biological molecules. Therefore, this chapter will show exciting results of the group using fluorescent proteins and nanocrystals in biological systems.

**Keywords:** nanocrystals, fluorescent proteins, fluorescent markers, magic-sized quantum dots, titanium dioxide

## 1. Introduction

Several types of tools have been developed in order to monitor biological processes through fluorescence images. Some of these tools are the use of fluorescent proteins and nanomaterials. This book chapter will comment in particular on green fluorescent protein and luminescent nanocrystals.

The green fluorescent protein (GFP) of Jellyfish *Aequoria victoria* and fluorescent homologous proteins of different colors isolated from other sea creatures have led to the development of fluorophores that have been widely used in recent

decades. In the biological area, fluorescent antibodies are a powerful tool for analyzing the subcellular location of proteins of interest. In addition, a gene encoding a fluorescent protein can be introduced into a model organism, resulting in the expression of functional fluorescent proteins, which can then be detected by fluorescence microscopy, flow cytometry, and other fluorescence-based methods. Fluorescent proteins have revolutionized biological and biomedical research, for example, it is possible to monitor the activity of a gene promoter by placing a fluorescent protein under its control. By using this tool, the spatial and temporal patterns of gene activation were revealed, as well as it was possible to trace the specific fates of cell populations or even to visualize the different shapes that cells can assume during development. Perhaps the most sophisticated area is the construction of genetically modified fluorescent sensors for the detection of ions, small molecules, and various types of enzyme activity [1–3].

One of the best and most used *in vivo* models to investigate biological phenomena is the fruit fly. The fruit fly *Drosophila melanogaster* is a well-established model organism in nanotoxicology studies [4]. *Drosophila* has a short life cycle, low maintenance cost, and a considerable amount of conserved genes and physiological mechanisms with humans [5, 6]. The complete sequencing of the *Drosophila* genome combined with genetic editing techniques allows the construction of reporter lines (for example, GFP) fused to specific genes [6]. One of the main tools that make the fruit fly an excellent model organism is the possibility of expressing genes of interest in specific tissues through the UAS-GAL4 binary expression system. This system consists of two factors: the GAL4 transcription factor fused to the promoter region of a gene of interest and the upstream activation sequence (UAS). GAL4 is able to bind the upstream activation sequence (UAS), activating the transcription of a target gene linked to UAS, allowing ectopic gene expression [6]. Thus, the use of fluorescent reporter genes under the control of the UAS-GAL4 system allows a degree of specificity necessary to monitor cellular and biochemical phenomena *in vivo* in different tissues, such as autophagy, [7] mitophagy [8], and changes in the redox state of cells [1]. Taken together, these features are essential for studies that evaluate the effects of xenobiotics on development, however, it can still be improved in the nanotoxicology area, mainly in the use of reporter lines for the elucidation of cellular mechanisms responsible for toxicity and the subcellular localization of nanocrystals.

The development of different nanoscale materials has increased for different applications. Titanium dioxide (TiO<sub>2</sub>) nanocrystals (NCs) have been used in several types of cosmetics, food, and the textile industry [9, 10]. This is because this NC has a wide variety of properties that improve materials, such as its bioluminescence and chemical stability [11]. Bioluminescent techniques are widely used in biomedicine for studies of drug screening, molecular markers, and monitoring of molecular reactions, among other applications [12]. Bioluminescent NCs, such as TiO<sub>2</sub>, present an excellent opportunity to obtain ultra-sensitive and enhanced analyzes and images, in addition to allowing the study of bioluminescence [13–15]. The use of bioluminescent imaging *in vivo* allows the visualization of biological processes in intact living organisms, providing abundant quantitative space–time information beyond the reach of conventional *in vitro* tests and fixed material [15].

Doping is a technique that allows the incorporation of substitutional ions into the crystalline structure of materials, generating exciting properties [16]. TiO<sub>2</sub> nanocrystals (NCs) with europium ions incorporated in their structure can be visualized in red fluorescence [17]. This acquired property makes it possible to track luminescence, thus being able to be coupled to biomolecules and drugs for studies of effects and tracking them, for example, which can assist in the studies of

quantitative monitoring of molecular reactions and cellular behaviors, allowing a better understanding of the functions dynamic and complicated biological phenomena [18, 19].

Quantum dots (QDs) of cadmium chalcogenides (CdSe, CdS, and CdTe) absorb and emit in the visible electromagnetic spectrum, and for this reason, they are used in several applications of biological and biomedical marking, such as fluorescent probes, biosensors, and others. In the area of biological labeling, the great applicability of QDs occurs because they present several advantages over traditional organic fluorophores, such as a long fluorescence life span, ~ 100 times greater, which allows to distinguish it from the background signal, seen that autofluorescence has a much shorter fluorescence life; absorption and emission spectra tunable; high photo resistance and chemo-degradation; and high fluorescence intensity [20–22]. However, this comparison of the fluorescence intensity of the QDs was performed in non-aqueous solvents, with unconjugated QDs, and in non-biological media, since the fluorescence intensity may be lower when the QDs are conjugated and used in biological labeling experiments [23].

Ultra-small PQs (USPQs) are nanocrystals with extremely small sizes, presenting strong quantum confinement effects, in which most of their atoms are located on the surface [24]. A large number of atoms on the surface and the presence of several pendant bonds lead to changes in the properties of nanocrystals, which can be observed in the fluorescence spectra [25].

The quantum dots of magic-sized (MSQDs) are nanocrystals with extremely small sizes (<2 nm) and that present physical property utterly different from traditional QDs [26]. Although MSQDs have similar properties to USQDs, including composition and size, some fundamental properties place these QDs in different classes. The characteristic properties of MSQDs are thermodynamically stable structures, wide luminescence range, high size stability over time, relatively narrow absorption spectra and/or heterogeneous (discontinuous) growth [27–31]. The structures are thermodynamically stable; they are formed from the arrangement of a certain number of atoms, which gives it high stability. Nguyen et al. made theoretical predictions of different types of CdSe MSQDs structures aligned with the literature's experimental results [32]. The term magic size is related to a (magic) number of atoms in the structure that makes QDs extremely stable [32]. The broad luminescence spectrum occurs due to MSQDs having internal atomic defects (absence or extra presence of atoms) [27, 29, 32].

The development of new alternatives for the study of biomolecules in organic systems has grown considerably. The high specificity and sensitivity of scientific methodologies based on fluorescence clarify biological events [33]. Fluorescent probes based on organic dyes have been shown to identify biomolecules [34, 35]. Silva et al. demonstrated that the biocompatibility of CdSe/CdS MSQRd could be tuned in the synthesis, [36] present high luminescence stability in biological systems [37], can be bioconjugated with several biomolecules aiming at the most diverse luminescent probes [38–42] and in biosensors [43, 44].

This chapter shows recent results that the group has been working with fluorescent reporter proteins and the applicability of nanocrystals as fluorescent markers. Nanocrystals of pure and europium doped TiO<sub>2</sub> and CdSe/CdS (MSQDs) will be some of the exciting tools for marking in biological systems.

## **2. Fluorescent proteins and nanocrystals**

This section will show the group results using GFP tagged proteins and nanocrystals' applicability as fluorescent markers.

## 2.1 *Drosophila* lines expressing fluorescent proteins

In 2011, Albrecht et al. established a monitoring system that allows assessing the status of chemically defined redox species (the redox pair GSH/GSSH and  $H_2O_2$ ) in subcellular compartments cytosol and mitochondria *in vivo*. They have fused a probe sensitive to redox changes (ro-GFP2) [45–47] to the microbial  $H_2O_2$  sensor oxidant receptor peroxidase 1 (Orp1) [46]. In a reduced state, this probe exhibits excitation around 488 nm, while upon oxidation, roGFP2 gains excitability at 405 nm and loses excitability at 488 nm. In the present work, we used one of the transgenic *Drosophila* lines described by Albrecht and collaborators, called mito-roGFP2-Orp1 [1] to exemplify how *in vivo* sensors can be valuable for analyzing the redox state and to propose its use for the analysis of nanomaterials biocompatibility *in vivo*. In **Figure 1** we show different dissected larval tissues of *Drosophila*

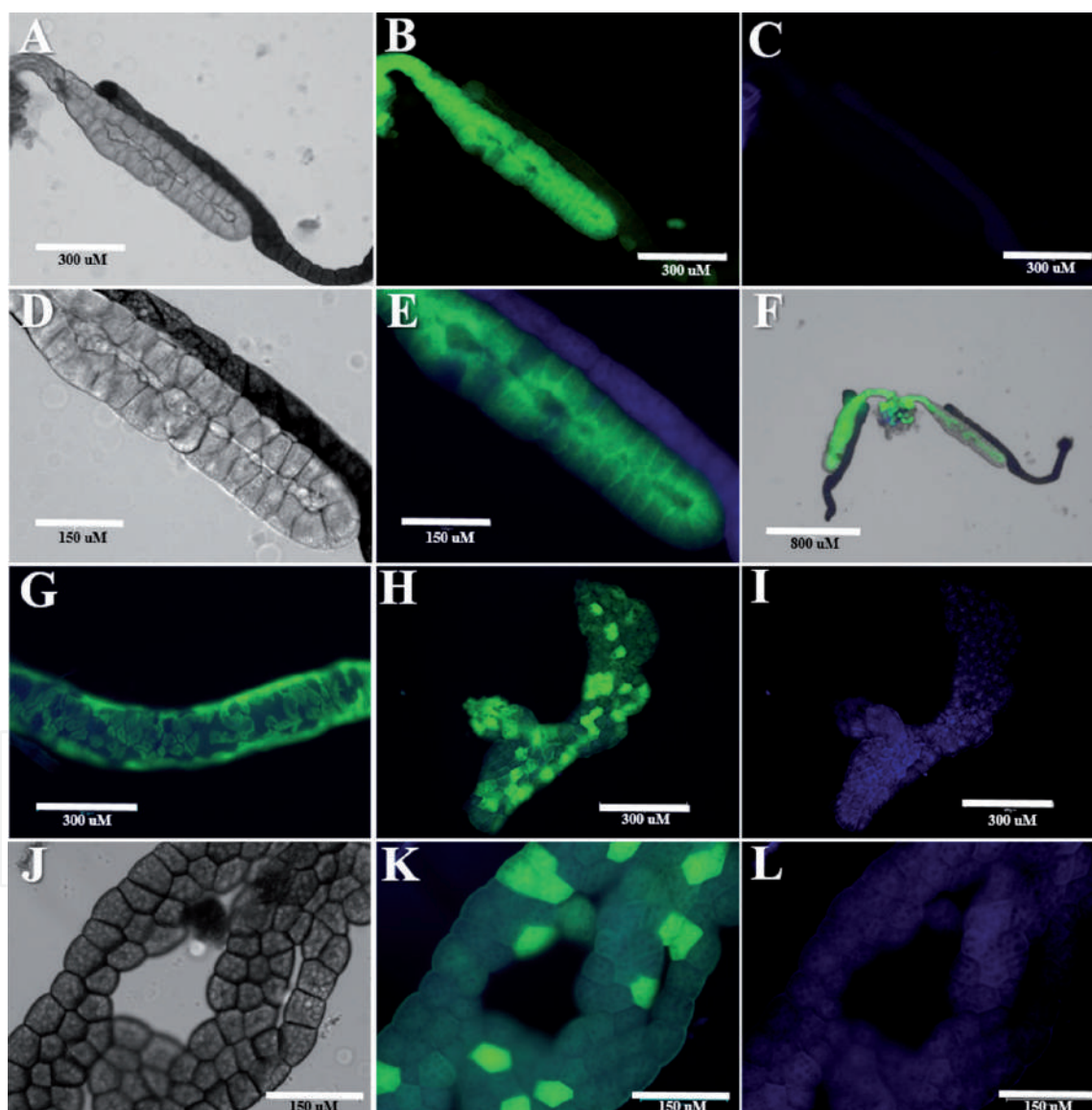


**Figure 1.**

*Drosophila* lines expressing fluorescent proteins can be used as *in vivo* sensors of redox status. Different GAL4 drivers were used to express Mito-orp1-GFP in different *Drosophila* larval tissues. (A-F) The *Drosophila* GAL4 driver *sgs3-GAL4* was used to express Mito-orp1-GFP2 in larval salivary glands. A- bright field image of a *Drosophila* larval salivary gland. In (B) the Mito-orp1-GFP can be visualized in its reduced state, while in (C) a weak signal is seen under 405 nm light. A greater magnification of the salivary gland shown in (A) can be seen in (D) while in (E) the overlap of the Mito-orp1-GFP2 in its reduced (488 nm) and oxidized (405 nm) state is shown. (G) Larval midgut showing the overlap of the Mito-orp1-GFP2 in its reduced (488 nm) and oxidized (405 nm) state. The Mito-orp1-GFP2 in its reduced state is shown in (H) and (K) while the sensor oxidized fluorescence is seen in (I) and (L). All images were acquired using ThermoFisher Scientific EVOS M7000 Imaging System.

expressing the redox sensor mito-roGFP2-Orp1. **Figure 1A** shows the bright field image of a dissected larval salivary gland, while in 3B we can see that there is a high concentration of mito-roGFP2-Orp1 in its reduced state, evidenced by green fluorescence, and a low concentration of mito-roGFP2-Orp1 in its oxidized state. In 1D, a higher magnification image of the salivary gland in 1A is shown, while in 1E the merged image of 488 nm and 405 nm channels shows the balance between reduced and oxidized mito-roGFP2-Orp1. In 1G, a portion of the midgut also shows a higher concentration of reduced mito-roGFP2-Orp1. **Figure 1H** shows reduced mito-roGFP2-Orp1 distribution throughout the larval fat body. It is interesting to notice that there is a clear difference in the concentration of reduced mito-roGFP2-Orp1 in cells within the same tissue, which is even more evident in the image in greater magnification shown in 1 K. The samples in 1I and 1 L show the oxidized mito-roGFP2-Orp1 in the same larval fat body. As expected, our analysis of control samples showed that most mito-roGFP2-Orp1 proteins are in its reduced state, exhibiting excitation around 488 nm. We are currently using this valuable tool to analyze the effect of different nanocrystals on the redox balance in *Drosophila* as an additional approach for the determination of biocompatibility *in vivo*.

**Figure 2** shows three different transgenic lines of *Drosophila* that can be used to assist in the subcellular localization of fluorescent nanoparticles. **Figure 2A-C** shows dissected tissues of the D1-GFP transgenic line (BL.66454). The D1-GFP protein binds to chromosomes allowing the nuclei visualization. In **Figure 2A** we can see a pair of larval salivary glands while **Figure 2B-C** shows different portions of the larval gut. The progeny of the cross between the lineage *mef2-Gal4* and *UAS-mito-GFP* (BL. 8443) was used to visualize the larval muscles (**Figure 2D-F**). This is because *mef2-Gal4* drives Gal4 expression in muscles where it binds to the regulatory sequence *UAS-mito-GFP*, which in turn regulates the expression of a

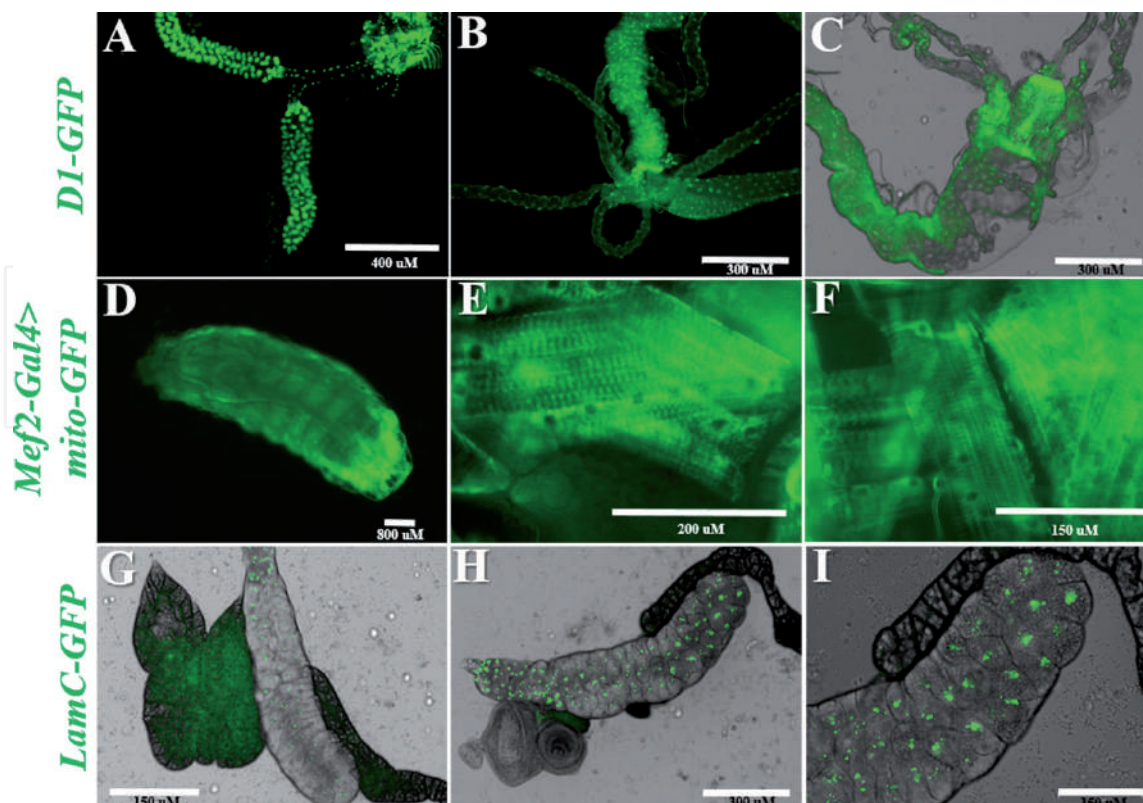


**Figure 2.** The expression of fluorescent proteins in *Drosophila* as a tool to visualize cellular subcompartments. (A-C) D1-GFP expression in *Drosophila* larval tissues. A pair of larval salivary glands is shown in (A) while (B) and (C) shows different portions of the larval gut. (D-F) L3 larvae expressing Mito-GFP in muscles. (G-I) shows salivary glands expressing LamC-GFP localization at the nuclear envelope of cells.

mitochondrial import sequence fused to the fluorescent protein GFP, allowing the visualization of mitochondria in the muscle tissues. **Figure 2G-I** shows salivary glands of the LamC-GFP transgenic lineage (BL. 6837) which allows for the visualization of the nuclear envelope of cells. In these examples, we showed 3 different *Drosophila* transgenic lines in the green band (GFP) that can be used to assist in the subcellular localization of fluorescent nanoparticles, however, it is essential to notice that hundreds of lines are available. Data on the genome and the wide range of reporter lines of *Drosophila* can be found on Flybase (<https://flybase.org/>). Reporter lines of *Drosophila* can be purchased in collections such as Bloomington *Drosophila* Stock Center (BDSC) at Indiana University. These different tools allow the investigators to choose from a great variety of cell types, subcellular compartments as well as the fluorescence band that best adapts to the nanoparticles of interest.

## 2.2 Nanocrystals as luminescent markers (nanomarkers)

**Figure 3** shows exciting results on pure and europium (Eu) doped TiO<sub>2</sub> NCs. TiO<sub>2</sub> NCs absorb and emit in the ultraviolet, but when incorporating the europium ions in its crystalline structure, by replacing some titanium ions, it shows luminescence in red. The colors emitted by the pure and Eu doped TiO<sub>2</sub> NCs (**Figure 3a**), and the crystalline structure in the anatase phase (**Figure 3b**) are illustrated. Also, in **Figure 3c**, the emission spectra of these nanocrystals are observed.

In order to investigate whether TiO<sub>2</sub> and TiO<sub>2</sub>:Eu nanocrystals could be tracked on adult *Drosophila* after exposure during development TiO<sub>2</sub> and TiO<sub>2</sub>:Eu nanocrystals were mixed in standard *Drosophila* culture medium at the final concentration of 100 mM. The larvae were carefully staged and transferred as L1 (first instar larvae) to medium containing TiO<sub>2</sub> and TiO<sub>2</sub>:Eu. The control contained only a standard *Drosophila* culture medium. The animals developed through all larval stages during the following 3 days. At this stage, the larvae actively feed until they become pupae. After pupal metamorphosis, the animals emerged as adults were dissected and its abdominal fat body was analyzed through fluorescence microscopy under UV light to analyze the TiO<sub>2</sub> bioaccumulation and under red light to detect TiO<sub>2</sub>:Eu. All samples images were acquired using the same light intensity and exposure time. **Figure 4** shows the tracking data of TiO<sub>2</sub> and TiO<sub>2</sub>:Eu in the fat body of adult animals after exposure during the larval stage. It is possible to observe that the fat body spheres of the control animals (**Figure 4A** and **C**) show intrinsic fluorescence when excited with ultraviolet light, however when the animals were exposed to TiO<sub>2</sub> the intensity of fluorescence was significantly higher (**Figure 4B** and **D**).

In order to distinguish between intrinsic fluorescence from fat body and TiO<sub>2</sub> fluorescence, the pixel intensity was measured and compared among all fat body spheres of control images and TiO<sub>2</sub> treated samples. As we can observe in the graphic in **Figure 5a** there was a drastic increase in fluorescence due to the presence of TiO<sub>2</sub>. The fat body spheres of the control animals (**Figure 4E** and **G**) also showed intrinsic fluorescence when excited with red light; however, when the animals have exposed to TiO<sub>2</sub>:Eu the intensity of fluorescence was higher (**Figure 4F** and **H**). The pixel intensity analysis showed that the presence of TiO<sub>2</sub>:Eu caused a significant increase in fluorescence (**Figure 5b**). The observation that the NCs of TiO<sub>2</sub> and TiO<sub>2</sub>:Eu could be detected in the fat body of newly emerged adult animals indicates that the bioaccumulation of nanocrystals during larval development persisted until the beginning of the adult stage. Surprisingly, we observed that animals dissected on the second day of its emergence no longer had fat bodies fluorescent spheres containing nanocrystals. This may indicate that one day following the emergence, the animals were able to excrete the NC. The disappearance of nanocrystals may

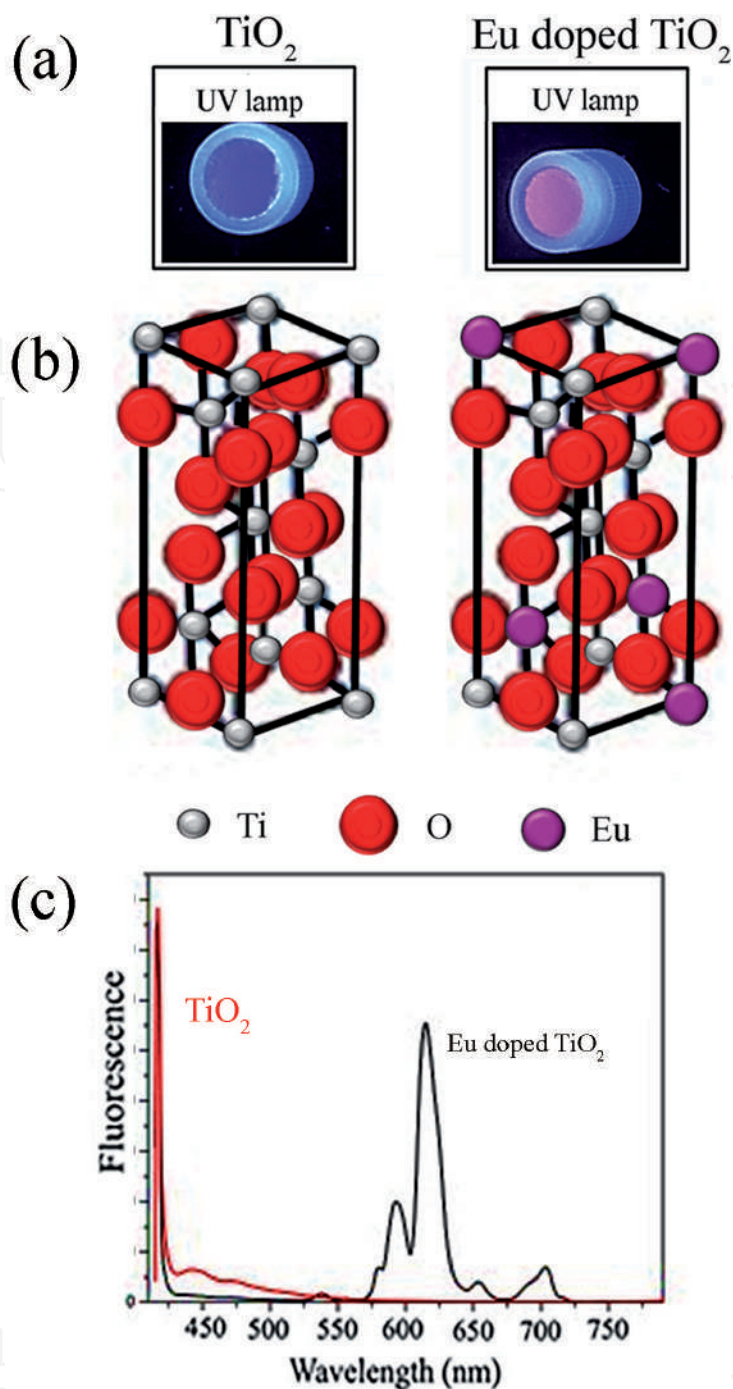


**Figure 3.** (a) Photographic image of nanopowders, (b) anatase crystalline structure, (c) luminescence spectra of pure and Eu doped  $\text{TiO}_2$  NCs.

also be related to the rapid absorption of the fat body during the first days of life. Similar results were described by Jovanovic et al. 2016, which observed that animals that received  $\text{TiO}_2$  during the larval stage did not have  $\text{TiO}_2$  as adults [9].

The optical properties and illustration of CdSe/CdS are shown in **Figure 6**. The aqueous solution and the illustration of the core/shell structure of CdSe/CdS MSQDs with a surfactant are exemplified to facilitate understanding (**Figure 6a, b**). The optical absorption and broad luminescence spectra are characteristics of magic-sized quantum dots of CdSe/CdS (**Figure 6c**). In addition, one of the essential properties of the CdSe/CdS MSQDs that allows its application in biological systems is entering and staying inside cells. To test this capacity, we incubated a classical macrophage cell line (RAW 264.7) with CdSe/CdS MSQDs of (200 ng/ $\mu\text{L}$ ) and evaluated their internalization by Flow Cytometry in different time points (1 to 60 minutes). Flow

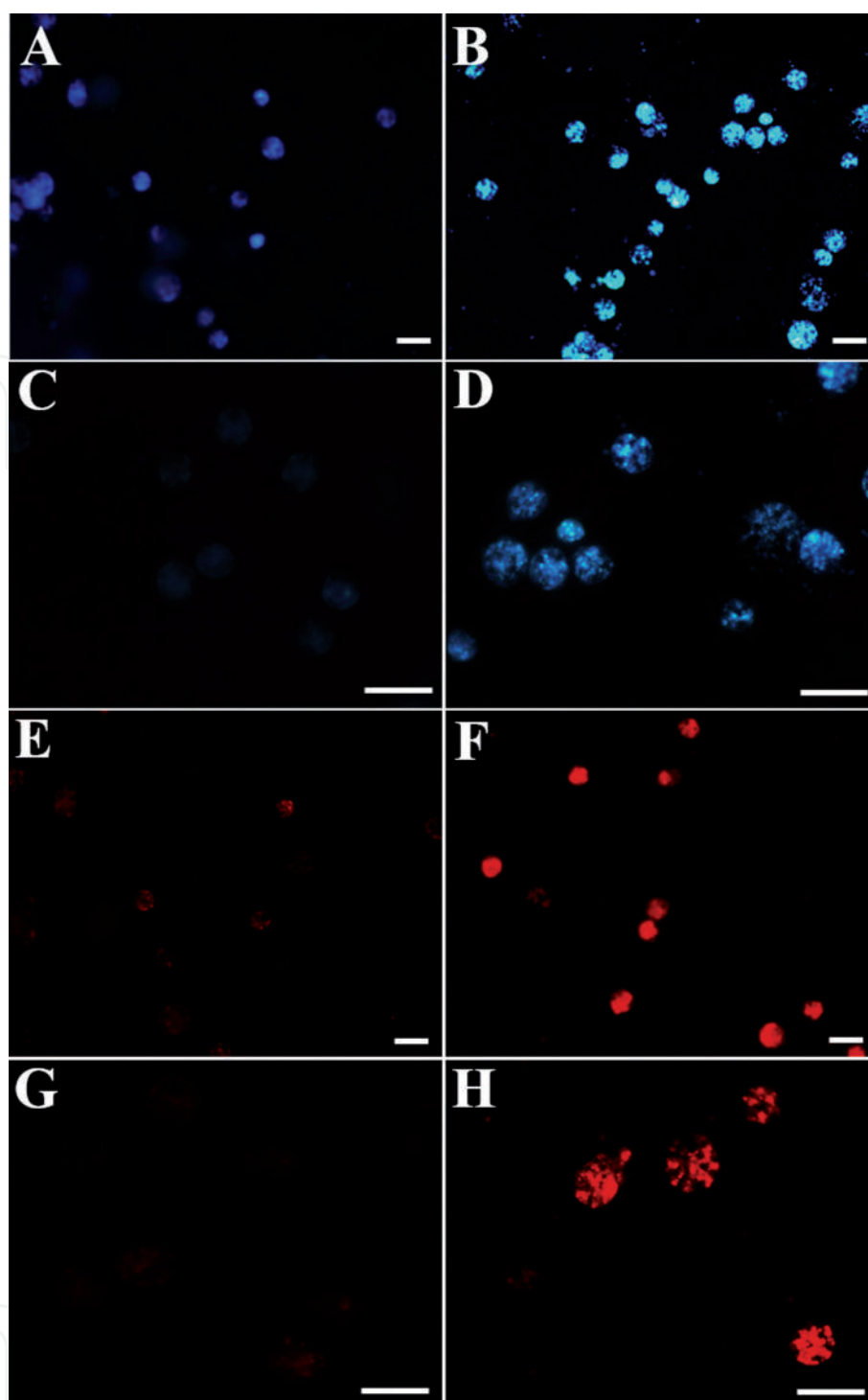


**Figure 4.** In vivo fluorescence of  $\text{TiO}_2$  and  $\text{TiO}_2:\text{Eu}$  in adult *Drosophila* fat body. *Drosophila* tissues as the fat body shows a well-known intrinsic fluorescence as observed in representative images of control animals (A) and (C) at 405 nm E and G at 546 nm), however in the  $\text{TiO}_2$  (B and D) and  $\text{TiO}_2:\text{Eu}$  (F and H) treated animals it is possible to observe a drastic increase in luminescence when compared to control. Scale bar represents 50 $\mu\text{M}$ .

Cytometry is a unique methodological approach to determine cell staining as it evaluates a considerable number of cells per second, one by one, and reports if cells are fluorescent. Just after 1 minute, the MSQDs nearly 50% of cells were fluorescent, and this percentual was growing to >97% after 60 minutes (**Figure 6c, d**).

Bioimaging assays are biological applications QDs since they can be bioconjugated with proteins, antibodies, and DNA [39, 48, 49]. In general, these tests depend on the biocompatibility of QDs, which is obtained by functionalizing the surface of these nanoparticles [39, 50–52]. The bioconjugation allows the study and tracking of biomolecules in biological systems such as cell cultures

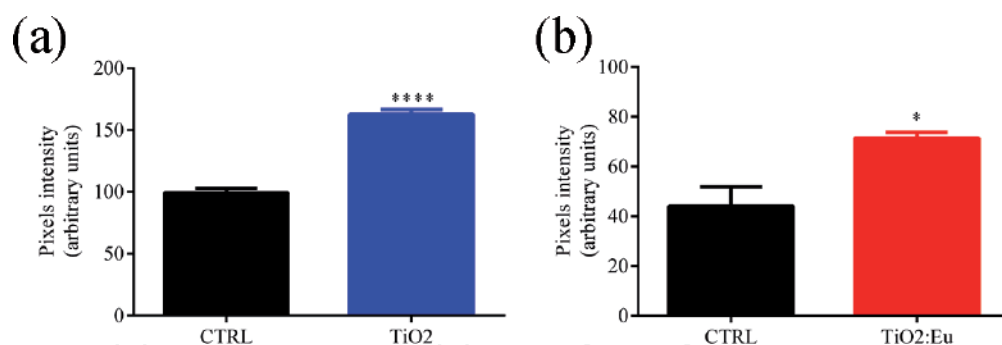


**Figure 5.** Indirect quantification of  $\text{TiO}_2$  and  $\text{TiO}_2:\text{Eu}$  fluorescence. (a) Pixel intensity analysis of fat body spheres of  $\text{TiO}_2$  treated *Drosophila* to control fat body spheres. (b) Pixel intensity analysis of fat body spheres of  $\text{TiO}_2:\text{Eu}$  treated animals compared to control fat body spheres.

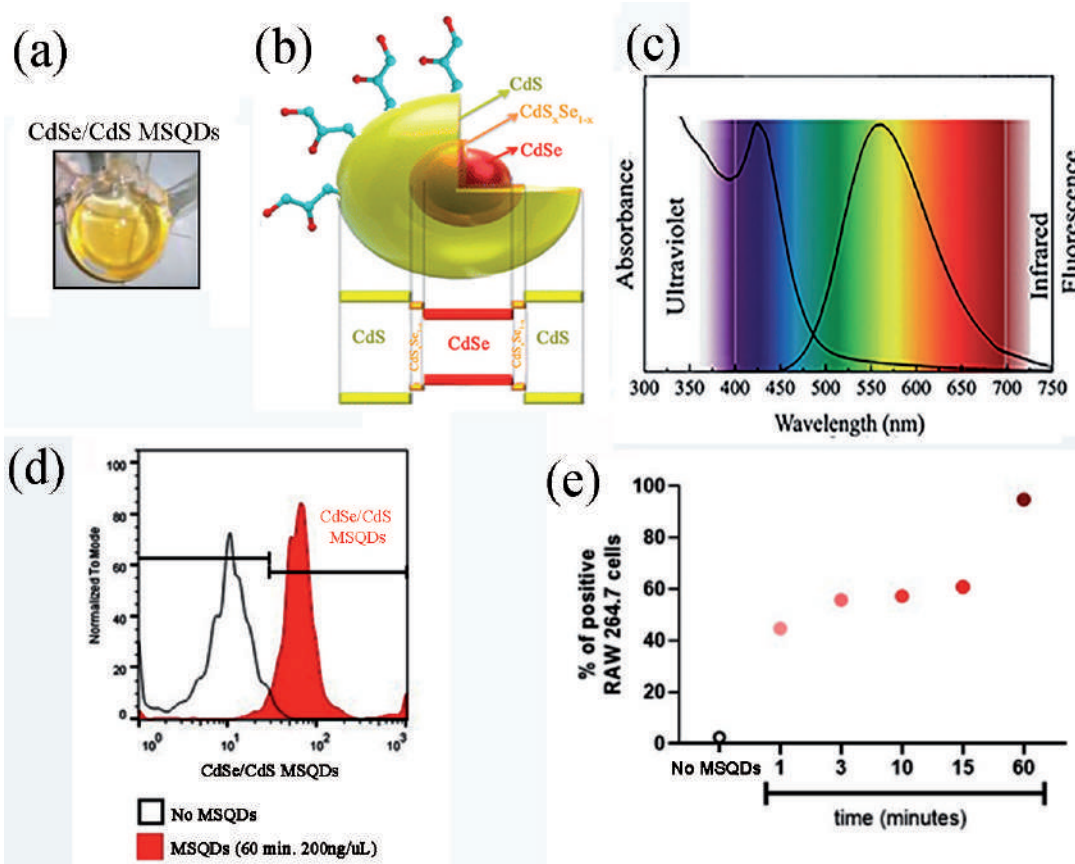


**Figure 6.** (a) Photographic image of solution, (b) illustration of CdSe/CdS MSQDs, (c) optical absorption/luminescence spectra of CdSe/CdS MSQDs (d, e) incorporation of MSQDs by RAW 264.7. The intracellular location was determined by flow cytometry after incubation of CdSe/CdS MSQDs (200 ng/uL) with RAW 264.7 cell line ( $1 \times 10^4$ /mL) at different time points. Cells were washed in saline solution before acquisition to exclude extracellular MSQDs. At least 5000 events were acquired in a FACS Calibur flow cytometer.

and laboratory animals [53, 54]. The versatility of QDs associated with maltose-binding protein for intracellular delivery of the drug beta-cyclodextrin [55]. Other studies have used the quantum dots for *in vivo* multiphoton biologic imaging. Kwon et al. conjugated iron selenide QDs with monoclonal human epidermal growth factor receptor 2 antibodies to study xenograft breast tumor model in mice [56].

The tracking and study of biomolecules labeled with QDs *in vitro* and *in vivo* is a reality in several areas, allowing us to analyze the location and distribution of bioconjugate in biological systems. Silva et al. demonstrated that the CdSe/CdS MSQDs could be bioconjugated with several biomolecules aiming at the most

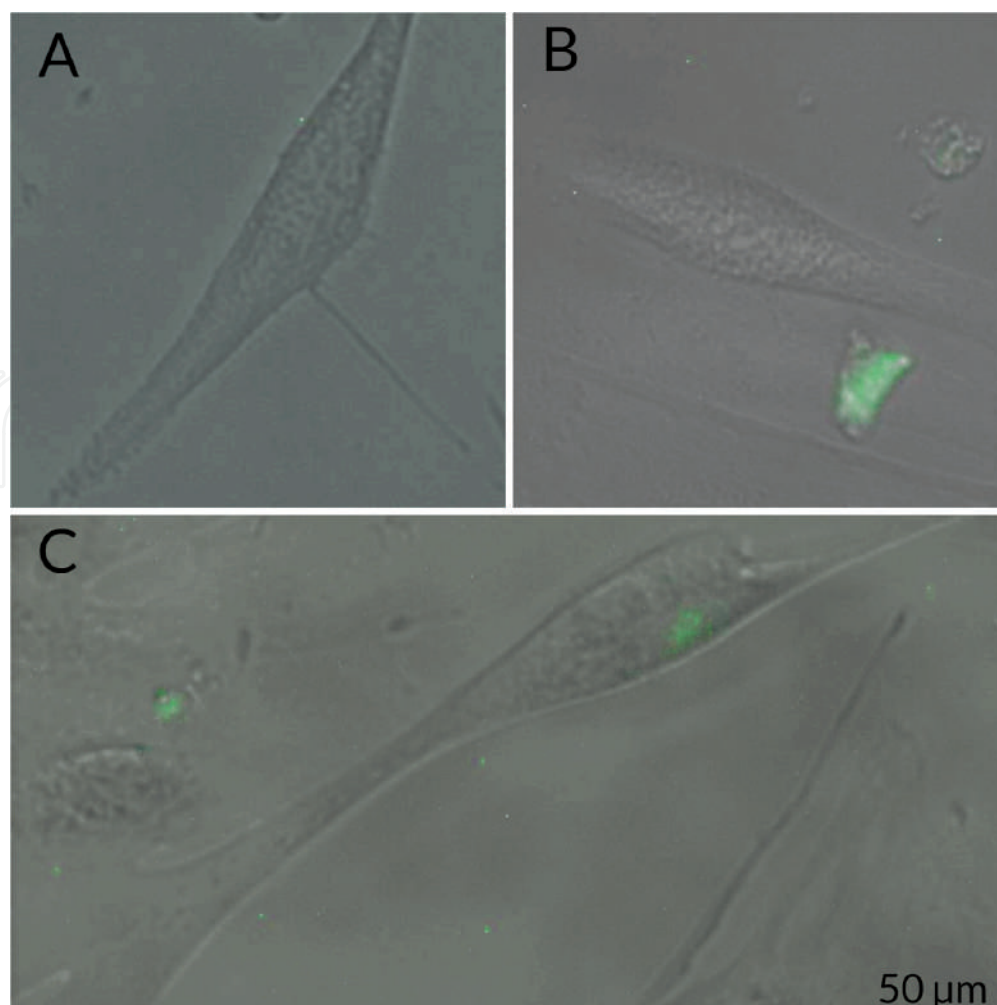


**Figure 7.**

Fluorescence microscopy images showing the tracking of BaltPLA<sub>2</sub> in myoblast culture. (A) Cell control (myoblasts only); (B) myoblasts treated with MSQDs (200 ng/μL) for 18 h; (C) myoblasts treated with MSQDs (200 ng/μL)-BaltPLA<sub>2</sub> (100 ng/μL) for 18 h. scale 50 μm.

diverse luminescent probes [38–42] in biosensors [43, 44]. Dias et al. labeled a phospholipase A2 isolated from *Bothrops alternatus* snake venom with CdSe/CdS MSQDs to track it in myoblast culture, making it possible to identify the bioconjugate on the surface of the plasma membrane and in the nuclear region [39]. **Figure 7** corroborates these data since it is possible to observe fluorescence markings only in myoblasts treated with the bioconjugate MSQDs-BaltPla2.

### 3. Conclusion

In this chapter, we have shown that fluorescent reporter proteins in the *Drosophila* model system are excellent tools to monitor cellular and biochemical phenomena *in vivo*, such as changes in the redox state of cells, as well as are a valuable tools to assist in the subcellular localization of fluorescent nanoparticles. We also showed that TiO<sub>2</sub> and Eu doped TiO<sub>2</sub> NCs fluorescence could be detected in adult animals following exposure during development. Intracellular location of CdSe/CdS MSQDs in RAW 264.7 cell line and tracking of BaltPLA<sub>2</sub> bioconjugated in myoblast culture. Therefore, the use of fluorescent proteins and nanocrystals *in vivo* are exciting tools as they provide abundant qualitative and quantitative data and allow the visualization of biological processes in intact cells and living organisms.

## **Acknowledgements**

This work was supported by grants of CNPq, CAPES, FAPEAL, and FAPEMIG.

## **Conflict of interest**

The authors declare no conflict of interest.

IntechOpen

IntechOpen

## Author details

Anielle Christine Almeida Silva<sup>1,2\*</sup>, Jerusa Maria de Oliveira<sup>3</sup>, Kelen Talita Romão da Silva<sup>1,3</sup>, Francisco Rubens Alves dos Santos<sup>1,3</sup>, João Paulo Santos de Carvalho<sup>1</sup>, Rose Kethelyn Souza Avelino<sup>3</sup>, Eurípedes Alves da Silva Filho<sup>4</sup>, Marcelo Duzzioni<sup>5</sup>, Edigar Henrique Vaz Dias<sup>6</sup>, Fábio de Oliveira<sup>7</sup>, Juliana Rodrigues Machado<sup>8</sup>, Malu Mateus Santos<sup>9</sup>, Marcos Vinícius da Silva<sup>9</sup>, Carlo José Freire de Oliveira<sup>9</sup>, Virmondés Rodrigues Junior<sup>9</sup>, Lucas Anhezini<sup>3</sup> and Noelio Oliveira Dantas<sup>1\*</sup>

1 Laboratory of New Nanostructured and Functional Materials, Physics Institute, Federal University of Alagoas, Maceió, Alagoas Brazil

2 Programa de Pós-Graduação da Rede Nordeste de Biotecnologia (RENORBIO), Federal University of Alagoas, Maceió, Alagoas Brazil

3 Laboratory for in vivo Toxicity, Institute of Biological Sciences and Health, Federal University of Alagoas, Maceió, Alagoas, Brazil

4 Laboratory of Genetic and Applied Microbiology, Institute of Biological Sciences and Health, Federal University of Alagoas, Maceió, Alagoas, Brazil

5 Laboratory of Pharmacological Innovation, Institute of Biological Sciences and Health, Federal University of Alagoas, Maceió, Alagoas, Brazil

6 State University of Minas Gerais, Ituiutaba, MG, Brazil

7 Institute of Biomedical Sciences, Federal University of Uberlândia, Uberlândia, MG, Brazil

8 Department of Pathology, Genetics and Evolution, Federal University of Triângulo Mineiro, Uberaba, Minas Gerais, Brazil

9 Department of Microbiology, Immunology, and Parasitology, Institute of Biological and Natural Sciences, Federal University of Triângulo Mineiro, Uberaba, MG, Brazil

\*Address all correspondence to: [aniellechristineas@gmail.com](mailto:aniellechristineas@gmail.com) and [noelio@fisufal.br](mailto:noelio@fisufal.br)

## IntechOpen

© 2021 The Author(s). Licensee IntechOpen. This chapter is distributed under the terms of the Creative Commons Attribution License (<http://creativecommons.org/licenses/by/3.0>), which permits unrestricted use, distribution, and reproduction in any medium, provided the original work is properly cited. 

## References

- [1] Albrecht, S.C.; Barata, A.G.; Großhans, J.; Teleman, A.A.; Dick, T.P. In vivo mapping of hydrogen peroxide and oxidized glutathione reveals chemical and regional specificity of redox homeostasis. *Cell Metab.* 2011, 14, 819-829, doi:10.1016/j.cmet.2011.10.010.
- [2] Chudakov, D.M.; Matz, M. V.; Lukyanov, S.; Lukyanov, K.A. Fluorescent proteins and their applications in imaging living cells and tissues. *Physiol. Rev.* 2010, 90, 1103-1163, doi:10.1152/physrev.00038.2009.
- [3] VanEngelenburg, S.B.; Palmer, A.E. Fluorescent biosensors of protein function. *Curr. Opin. Chem. Biol.* 2008, 12, 60-65, doi:10.1016/j.cbpa.2008.01.020.
- [4] Ong, C.; Yung, L.Y.L.; Cai, Y.; Bay, B.H.; Baeg, G.H. *Drosophila melanogaster* as a model organism to study nanotoxicity. *Nanotoxicology* 2015, 9, 396-403, doi:10.3109/17435390.2014.940405.
- [5] Pandey, U.B.; Nichols, C.D. Human disease models in *Drosophila melanogaster* and the role of the fly in therapeutic drug discovery. *Pharmacol. Rev.* 2011, 63, 411-436, doi:10.1124/pr.110.003293.
- [6] Hales, K.G.; Korey, C.A.; Larracuenta, A.M.; Roberts, D.M. Genetics on the fly: A primer on the drosophila model system. *Genetics* 2015, 201, 815-842, doi:10.1534/genetics.115.183392.
- [7] Devorkin, L.; Gorski, S.M. Monitoring autophagy in drosophila using fluorescent reporters in the UAS-GAL4 system. *Cold Spring Harb. Protoc.* 2014, 2014, 967-972, doi:10.1101/pdb.prot080341.
- [8] Kim, Y.Y.; Um, J.H.; Yoon, J.H.; Kim, H.; Lee, D.Y.; Lee, Y.J.; Jee, H.J.; Kim, Y.M.; Jang, J.S.; Jang, Y.G.; et al. Assessment of mitophagy in mt-Keima *Drosophila* revealed an essential role of the PINK1-Parkin pathway in mitophagy induction in vivo. *FASEB J.* 2019, 33, 9742-9751, doi:10.1096/fj.201900073R.
- [9] Jovanović, B.; Jovanović, N.; Cvetković, V.J.; Matic, S.; Stanić, S.; Whitley, E.M.; Mitrović, T.L. The effects of a human food additive, titanium dioxide nanoparticles E171, on *Drosophila melanogaster* - a 20 generation dietary exposure experiment. *Sci. Rep.* 2018, 8, 1-12, doi:10.1038/s41598-018-36174-w.
- [10] Chen, X.; Mao, S.S. Titanium dioxide nanomaterials: Synthesis, properties, modifications and applications. *Chem. Rev.* 2007, 107, 2891-2959.
- [11] Kamat, P. V. *Journal of Physical Chemistry C.* 2012, pp. 11849-11851.
- [12] Fleiss, A.; Sarkisyan, K.S. A brief review of bioluminescent systems (2019). *Curr. Genet.* 2019, 65, 877-882, doi:10.1007/s00294-019-00951-5.
- [13] Duarte, C.A.; Goulart, L.R.; Filice, letícia de S.C.; De Lima, I.L.; Campos-Fernandes, E.; Dantas, N.O.; Silva, A.C.A.; Soares, M.B.P.; Santos, R.R.; Cardoso, C.M.A.; et al. Characterization of Crystalline Phase of TiO<sub>2</sub>. *Materials (Basel)*. 2020, 13, 4071.
- [14] Barkalina, N.; Charalambous, C.; Jones, C.; Coward, K. Nanotechnology in reproductive medicine: Emerging applications of nanomaterials. *Nanomedicine Nanotechnology, Biol. Med.* 2014, 10, e921-e938, doi:10.1016/j.nano.2014.01.001.
- [15] Padmanabhan, P.; Kumar, A.; Kumar, S.; Chaudhary, R.K.; Gulyás, B. Nanoparticles in practice for molecular-imaging applications: An overview. *Acta*

*Biomater.* 2016, 41, 1-16, doi:10.1016/j.actbio.2016.06.003.

[16] Bharat, T.C.; Shubham; Mondal, S.; Gupta, H.S.; Singh, P.K.; Das, A.K. Synthesis of doped zinc oxide nanoparticles: A review. In *Proceedings of the Materials Today: Proceedings*; Elsevier Ltd, 2019; Vol. 11, pp. 767-775.

[17] Sandoval, S.; Yang, J.; Alfaro, J.G.; Liberman, A.; Makale, M.; Chiang, C.E.; Schuller, I.K.; Kummel, A.C.; Trogler, W.C. Europium-doped TiO<sub>2</sub> hollow nanoshells: Two-photon imaging of cell binding. *Chem. Mater.* 2012, 24, 4222-4230, doi:10.1021/cm302642g.

[18] Ghaderi, S.; Ramesh, B.; Seifalian, A.M. Fluorescence nanoparticles “quantum dots” as drug delivery system and their toxicity: A review. *J. Drug Target.* 2011, 19, 475-486, doi:10.3109/1061186X.2010.526227.

[19] Vollrath, A.; Schubert, S.; Schubert, U.S. Fluorescence imaging of cancer tissue based on metal-free polymeric nanoparticles-a review. *J. Mater. Chem. B* 2013, 1, 1994-2007, doi:10.1039/c3tb20089b.

[20] Alivisatos, P. The use of nanocrystals in biological detection. *Nat. Biotechnol.* 2004, 22, 47-52, doi:10.1038/nbt927.

[21] Resch-Genger, U.; Grabolle, M.; Cavaliere-Jaricot, S.; Nitschke, R.; Nann, T. Quantum dots versus organic dyes as fluorescent labels. *Nat Methods.* 2008, 5, 763-75.

[22] Deerinck, T.J. The application of fluorescent quantum dots to confocal, multiphoton, and electron microscopic imaging. *Toxicol. Pathol.* 2008, 36, 112-6, doi:10.1177/0192623307310950.

[23] Wu, X.; Liu, H.; Liu, J.; Haley, K.N.; Treadway, J.A.; Larson, J.P.; Ge, N.; Peale, F.; Bruchez, M.P. Immunofluorescent labeling of cancer marker Her2 and other cellular targets

with semiconductor quantum dots. *Nat. Biotechnol.* 2002, 21, 41-46.

[24] Dai, Q.; Li, D.; Chang, J.; Song, Y.; Kan, S.; Chen, H.; Zou, B.; Xu, W.; Xu, S.; Liu, B.; et al. Facile synthesis of magic-sized CdSe and CdTe nanocrystals with tunable existence periods. *Nanotechnology* 2007, 18, 405603, doi:10.1088/0957-4484/18/40/405603.

[25] Murray, C.B.; Kagan, C.R.; Bawendi, M.G. Synthesis and Characterization of Monodisperse Nanocrystals and Close-Packed Nanocrystal Assemblies. *Annu. Rev. Mater.* 2000, 30, 545.

[26] Chen, X.; Samia, A.C.S.; Lou, Y.; Burda, C. Investigation of the crystallization process in 2 nm CdSe quantum dots. *J. Am. Chem. Soc.* 2005, 127, 4372-4375, doi:10.1021/ja0458219.

[27] Riehle, F.S.; Bienert, R.; Thomann, R.; Urban, G.A. Blue Luminescence and Superstructures from Magic Size Clusters of CdSe. *Nano Lett.* 2009, 9, 514-518, doi:10.1021/nl080150o.

[28] McBride, J.R.; Dukes, A.D.; Schreuder, M. a; Rosenthal, S.J. On Ultrasmall Nanocrystals. *Chem. Phys. Lett.* 2010, 498, 1-9, doi:10.1016/j.cplett.2010.08.052.

[29] Dukes, A.D.; McBride, J.R.; Rosenthal, S.J. Synthesis of Magic-Sized CdSe and CdTe Nanocrystals with Diisooctylphosphinic Acid. *Chem. Mater.* 2010, 22, 6402-6408, doi:10.1021/cm102370a.

[30] Bowers, M.J.; McBride, J.R.; Rosenthal, S.J. White-light emission from magic-sized cadmium selenide nanocrystals. *J Am Chem Soc* 2005, 127, 15378-15379.

[31] Harrell, S.M.; McBride, J.R.; Rosenthal, S.J. Synthesis of ultrasmall and magic-sized CdSe nanocrystals. *Chem. Mater.* 2013, 25, 1199-1210.

- [32] Nguyen, K.A.; Day, P.N.; Pachter, R. Understanding structural and optical properties of nanoscale CdSe magic-size quantum dots: Insight from computational prediction. *J. Phys. Chem. C* 2010, *114*, 16197-16209, doi:10.1021/jp103763d.
- [33] Shashkova, S.; Leake, M.C. Single-molecule fluorescence microscopy review: Shedding new light on old problems. *Biosci. Rep.* 2017, *37*, BSR20170031, doi:10.1042/BSR20170031.
- [34] Martynov, V.I.; Pakhomov, A.A.; Popova, N. V.; Deyev, I.E.; Petrenko, A.G. Synthetic Fluorophores for Visualizing Biomolecules in Living Systems. *Acta Naturae* 2016, *8*, 33-46, doi:10.32607/20758251-2016-8-4-33-46.
- [35] Yan, F.; Fan, K.; Bai, Z.; Zhang, R.; Zu, F.; Xu, J.; Li, X. Fluorescein applications as fluorescent probes for the detection of analytes. *TrAC - Trends Anal. Chem.* 2017, *97*, 15-35, doi:10.1016/j.trac.2017.08.013.
- [36] Almeida Silva, A.; Silva, M.J.; da Luz, F.A.; Silva, D.; de Deus, S.; Dantas, N. Controlling the Cytotoxicity of CdSe Magic-Sized Quantum Dots as a Function of Surface Defect Density. *Nano Lett.* *14*, 5452-5457, doi:10.1021/nl5028028.
- [37] Silva, A.C.A.; Deus, S.L.V. De; Silva, M.J.B.; Dantas, N.O. Highly stable luminescence of CdSe magic-sized quantum dots in HeLa cells. *Sensors Actuators, B Chem.* 2014, *191*, 108-114, doi:10.1016/j.snb.2013.09.063.
- [38] Silva, A.C.A.; Dantas, N.O.; Silva, M.J.B.; Spanó, A.M.; Goulart, ; Luiz Ricardo Functional Nanocrystals : Towards Biocompatibility , Nontoxicity and. In *Advances in Biochemistry & Applications in Medicine*; 2017; pp. 1-27.
- [39] Dias, E.H.V.; Pereira, D.F.C.; de Sousa, B.B.; Matias, M.S.; de Queiroz, M.R.; Santiago, F.M.; Silva, A.C.A.; Dantas, N.O.; Santos-Filho, N.A.; de Oliveira, F. In vitro tracking of phospholipase A 2 from snake venom conjugated with magic-sized quantum dots. *Int. J. Biol. Macromol.* 2019, *122*, 461-468, doi:10.1016/j.ijbiomac.2018.10.185.
- [40] Silva, A.C.A.; Correia, L.IV.; Silva, M.J.B.; Zóia, M.A.P.; Azevedo, F.V.PV.; Rodrigues, Jéssica Peixoto Goulart, L.R.; Ávila, Veridiana de Melo Dantas, N.O. Biocompatible Magic Sized Quantum Dots: Luminescent Markers and Probes. In; Correia, L.IV., Ed.; IntechOpen: Rijeka, 2018; p. Ch. 6 ISBN 978-1-78923-295-0.
- [41] Silva, A.C.A.; Azevedo, F.V.PV.; Zóia, M.A.P.; Rodrigues, J.P.; Dantas, N.O.; Melo, V.R.Á.; Goulart, L.R. Magic Sized Quantum Dots as a Theranostic Tool for Breast Cancer. In *Recent Studies & Advances in Breast Cancer*; Open Access eBooks: Wilmington, 2017; pp. 1-10 ISBN 978-81-935757-2-7.
- [42] Silva, A.C.A.; Neto, E.S.F.; Da Silva, S.W.; Morais, P.C.; Dantas, N.O. Modified phonon confinement model and its application to CdSe/ CdS core-shell magic-sized quantum dots synthesized in aqueous solution by a new route. *J. Phys. Chem. C* 2013, doi:10.1021/jp308500r.
- [43] de França, C.C.L.; Meneses, D.; Silva, A.C.A.; Dantas, N.O.; de Abreu, F.C.; Petroni, J.M.; Lucca, B.G. Development of novel paper-based electrochemical device modified with CdSe/CdS magic-sized quantum dots and application for the sensing of dopamine. *Electrochim. Acta* 2021, *367*, 137486, doi:10.1016/j.electacta.2020.137486.
- [44] de Lima França, C.C.; da Silva Terto, E.G.; Dias-Vermelho, M. V.; Silva, A.C.A.; Dantas, N.O.; de Abreu, F.C. The electrochemical behavior of core-shell CdSe/CdS magic-sized

quantum dots linked to cyclodextrin for studies of the encapsulation of bioactive compounds. *J. Solid State Electrochem.* 2016, 20, 2533-2540, doi:10.1007/s10008-016-3221-8.

[45] Dooley, C.T.; Dore, T.M.; Hanson, G.T.; Jackson, W.C.; Remington, S.J.; Tsien, R.Y. Imaging dynamic redox changes in mammalian cells with green fluorescent protein indicators. *J. Biol. Chem.* 2004, 279, 22284-22293, doi:10.1074/jbc.M312847200.

[46] Gutscher, M.; Pauleau, A.L.; Marty, L.; Brach, T.; Wabnitz, G.H.; Samstag, Y.; Meyer, A.J.; Dick, T.P. Real-time imaging of the intracellular glutathione redox potential. *Nat. Methods* 2008, 5, 553-559, doi:10.1038/nmeth.1212.

[47] Hanson, G.T.; Aggeler, R.; Oglesbee, D.; Cannon, M.; Capaldi, R.A.; Tsien, R.Y.; Remington, S.J. Investigating Mitochondrial Redox Potential with Redox-sensitive Green Fluorescent Protein Indicators. *J. Biol. Chem.* 2004, 279, 13044-13053, doi:10.1074/jbc.M312846200.

[48] Silva, A.C.A.; Correia, L.I.V.; Silva, M.J.B.; Zóia, M.A.P.; Azevedo, F.V.P.V.; Rodrigues, J.P.; Goulart, L.R.; Ávila, Veridiana de Melo Dantas, N.O. Biocompatible Magic Sized Quantum Dots: Luminescent Markers and Probes. In *State of the Art in Nano-Bioimaging*; 2017; Vol. 1, pp. 95-104 ISBN 9789537619992.

[49] Silva, A.C.A.; Azevedo, F.V.P.V.; Zóia, M.A.P.; Rodrigues, J.P.; Dantas, N.O.; Melo, V.R.Á.; Goulart, L.R. Magic Sized Quantum Dots as a Theranostic Tool for Breast Cancer. In *Recent Studies & Advances in Breast Cancer*; 2017 ISBN 978-81-935757-2-7.

[50] Silva, A.C.A.; Freschi, A.P.P.; Rodrigues, C.M.; Matias, B.F.; Maia, L.P.; Goulart, L.R.; Dantas, N.O. Biological analysis and imaging applications of CdSe/Cd<sub>x</sub>Se<sub>1-x</sub>/CdS core-shell magic-sized quantum dot.

*Nanomedicine Nanotechnology, Biol. Med.* 2016, 12, 1421-1430, doi:10.1016/j.nano.2016.01.001.

[51] Vlasceanu, G.; Grumezescu, A.M.; Gheorghe, I.; Chifiriuc, M.C.; Holban, A.M. Quantum dots for bioimaging and therapeutic applications. In *Nanostructures for Novel Therapy: Synthesis, Characterization and Applications*; Elsevier Inc., 2017; pp. 497-515 ISBN 9780323461481.

[52] Li, J.; Wu, D.; Miao, Z.; Zhang, Y. Preparation of Quantum Dot Bioconjugates and their Applications in Bio-Imaging. *Curr. Pharm. Biotechnol.* 2010, 11, 662-671, doi:10.2174/138920110792246582.

[53] Gondim, B.L.C.; da Silva Catarino, J.; de Sousa, M.A.D.; de Oliveira Silva, M.; Lemes, M.R.; de Carvalho-Costa, T.M.; de Lima Nascimento, T.R.; Machado, J.R.; Rodrigues, V.; Oliveira, C.J.F.; et al. Nanoparticle-Mediated Drug Delivery: Blood-Brain Barrier as the Main Obstacle to Treating Infectious Diseases in CNS. *Curr. Pharm. Des.* 2019, 25, 3983-3996, doi:10.2174/1381612825666191014171354.

[54] Makride, S.C.; Gasbarro, C.; Bello, J.M. Bioconjugation of quantum dot luminescent probes for Western blot analysis. *Biotechniques* 2005, 39, 501-506, doi:10.2144/000112004.

[55] Field, L.D.; Walper, S.A.; Susumu, K.; Lasarte-Aragones, G.; Oh, E.; Medintz, I.L.; Delehanty, J.B. A Quantum Dot-Protein Bioconjugate That Provides for Extracellular Control of Intracellular Drug Release. *Bioconjug. Chem.* 2018, 29, 2455-2467, doi:10.1021/acs.bioconjchem.8b00357.

[56] Kwon, J.; Jun, S.W.; Choi, S.I.; Mao, X.; Kim, J.; Koh, E.K.; Kim, Y.H.; Kim, S.K.; Hwang, D.Y.; Kim, C.S.; et al. FeSe quantum dots for in vivo multiphoton biomedical imaging. *Sci. Adv.* 2019, 5, doi:10.1126/sciadv.aay0044.

# We are IntechOpen, the world's leading publisher of Open Access books Built by scientists, for scientists

6,300

Open access books available

171,000

International authors and editors

190M

Downloads

Our authors are among the

154

Countries delivered to

TOP 1%

most cited scientists

12.2%

Contributors from top 500 universities



WEB OF SCIENCE™

Selection of our books indexed in the Book Citation Index  
in Web of Science™ Core Collection (BKCI)

Interested in publishing with us?  
Contact [book.department@intechopen.com](mailto:book.department@intechopen.com)

Numbers displayed above are based on latest data collected.  
For more information visit [www.intechopen.com](http://www.intechopen.com)



# Design of Coelenterazine Analogue to Reveal Bioluminescent Reaction of Human Serum Albumin

Ryo Nishihara, Kazuki Niwa, Tatsunosuke Tomita  
and Ryoji Kurita

## Abstract

This chapter describes the design of an imidazopyrazinone-type luciferin named as HuLumino1 by us and investigation of its luminescence properties. This luciferin was designed to generate bioluminescence by human serum albumin (HSA) rather than by luciferase derived from luminous organisms. HuLumino1 was developed by modifying a methoxy-terminated alkyl chain to the C-6 position and eliminating a benzyl group at the C-8 position of coelenterazine. To clarify the basis of light emission by HSA, the detailed kinetic properties of the HuLumino1/HSA pair were investigated using a calibrated luminometer. The enzymatic oxidation of HuLumino1 was observed only in the presence of HSA. Results of HSA quantification experiments using HuLumino1 agreed with less than 5% differences with those of enzyme-linked immunosorbent assays, suggesting HuLumino1 could be used for quantitative analysis of HSA levels in serum samples without any pretreatments. These results demonstrate the advantages of the coelenterazine analogue as a bioluminescence reagent to detect non-labeled proteins, which generally do not function as enzymes.

**Keywords:** Bioluminescence, Coelenterazine, Luciferin, Luciferase, Human serum albumin, Quantum yield, Enzyme-linked immunosorbent assay

## 1. Introduction

Luminous organisms, such as *fireflies*, *Gaussia princeps*, *Oplophorus gracilirostris*, and *sea pansy Renilla reniformis*, generate bioluminescence (BL), which is the light emission in the absence of external energy sources [1, 2]. In the core of BL, an enzymatic reaction occurs involving a bioluminescent substrate (luciferin) and enzyme (luciferase). In general, the enzymatic luminescence reaction proceeds between a specific luciferin-luciferase pair to allow for highly sensitive and specific detection/imaging of diverse molecular events in living subjects [2–4].

However, in some cases, bioluminescent or chemiluminescent substrates may induce enzymatic luminescence activity of non-bioluminescence enzymes. For example, CycLuc2, a synthetic analog of firefly luciferin, can be catalyzed to emit light by long-chain fatty acid acyl-CoA synthetase found in non-luminous insects

[5–7]. In addition, the heme-containing enzyme myeloperoxidase, which is abundantly expressed in neutrophils and monocytes, can catalyze the luminescence reaction of xenobiotic luminol [8, 9]. These reports suggested that the introduction of appropriate exogenous luminescent substrates reveals luminous activity of non-bioluminescence enzymes, which can significantly differ from the conventional function of the enzyme and has potential for use in quantitative analysis of enzymes without any labeling procedures, including transgene introduction of luciferase from luminous organisms. Here, we describe the design and bioluminescence characterization of a luciferin analogue which was selectively catalyzed to exhibit bioluminescence by human serum albumin (HSA) [10]. Serum albumins perform various physiological functions; they maintain colloid osmotic blood pressure and transport several exogenous and endogenous molecules. However, they are not categorized in the list of EC number, indicating they are not considered typical enzymes. The bioluminescence system of HSA with the luciferin analogue synthesized by us is novel and different from the conventional luciferin-luciferase reaction systems.

## 2. Design of coelenterazine analogue

### 2.1 Coelenterazine analogue with HSA-specific bioluminescence

Most luciferases from luminous marine organisms use coelenterazine (CTZ) as their luciferin to form coelenteramide in an excited state, with emission ranging from blue to green at approximately 400–500 nm (**Figure 1**) [11, 12]. CTZ is oxidized by bovine serum albumin (BSA) in addition to luciferase, and this has been considered as nonspecific reaction mainly occurs because of a simple luminescence reaction that requires only an oxygen molecule [1] (**Figure 1**).

The emission ability of CTZ is derived from the imidazopyrazinone ring, and the chemical structure of sidechains at the C-2, C-6, and C-8 position of the imidazopyrazinone core significantly affect enzyme recognition. For example, *Cypridina* luciferase oxidizes only *Cypridina* luciferin, which contains a basic guanidine moiety at the C-8 position of the imidazopyrazinone ring, not CTZ (**Figure 2**) [13]. A mutant *Oplophorus* luciferase (NanoLuc) uses furimazine rather than CTZ, and is known as a versatile reporter of BL (**Figure 2**) [14]. Thus, each bioluminescence probe has been individually developed with an imidazopyrazinone analogue that is suitable for the geometry of the active site in the pocket of mutant luciferase. We also reported that RLuc8.6-535SG, a mutant *R. reniformis* luciferase, utilizes BottleBlue2.3 (BBlue2.3), a CTZA that can permeate the cell membrane and emits bright visible luminescence suitable for deep-tissue imaging of cancer cells in vivo (**Figure 3a**) [15].

To clarify the potential enzymatic luminescence activity of human proteins, we focused on HSA, which accounts for approximately 65% of serum proteins in the human body [16]. This abundant protein is involved in a wide variety of

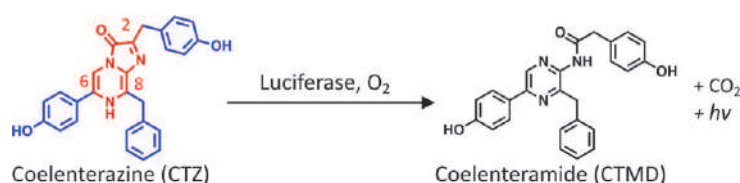


**Figure 1.**

Chemical reaction of coelenterazine (CTZ)-dependent bioluminescence. The imidazopyrazinone structure and modifiable substituent are highlighted in red and blue, respectively.

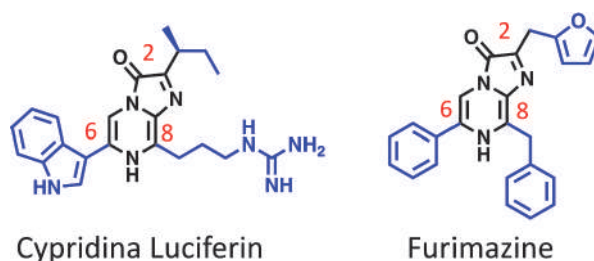


**Figure 2.**  
 Chemical structures of imidazopyrazinone-based analogues.

**(a) Chemical structures of CTZ analogues with C-2 and/or C-6 modifications**

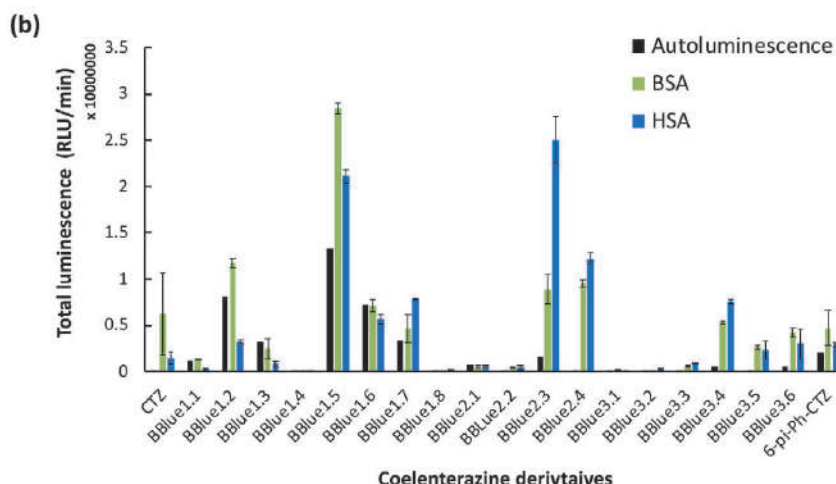
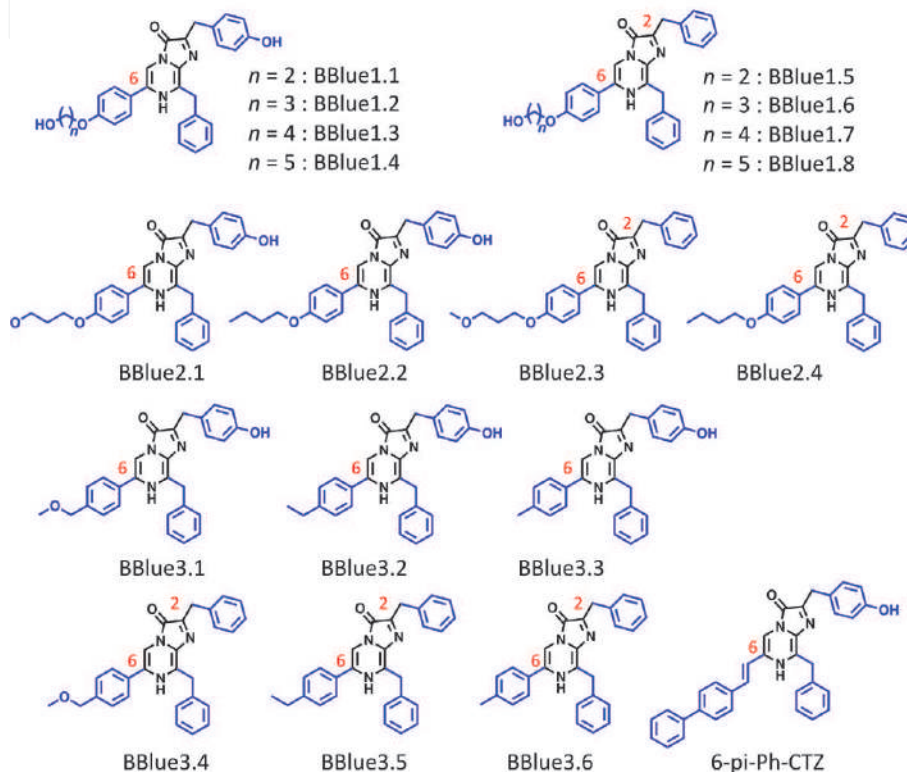


**Figure 3.**  
 Chemical structures of coelenterazine analogues (CTZAs) upon (a) C-2 and/or C-6 substitution.  
 (b) Luminescence intensities obtained with serum albumin (0.1 mg/mL).

physiological functions, such as maintaining osmotic pressure, buffering blood pH levels, and carrying ligands including hormones, amino acids, and fatty acids [17, 18]. In addition, HSA and some ligand complexes often possess enzymatic activities, such as Kemp elimination and hydrolysis of esters because of their unique

ability to bind small hydrophobic molecules in some cavities; however, the potential enzymatic activities remain unclear [17, 19].

First, to obtain a rational luciferin with an imidazopyrazinone core for HSA-specific BL, we assayed CTZ and previously reported 18 CTZAs named as Bottle Blue (BBlue), where the *p*-hydroxy phenyl group at the C-6 position of CTZ was modified by alkylation (**Figure 3**), with serum albumins (fatty acid free HSA and BSA). In this chapter, except for in Section 2.2, luminescence measurements were performed using luminometers (GloMax20/20 Luminometer or GloMax Explorer Multimode Microplate Reader) manufactured by Promega (Madison, WI, USA). Next, BBlue2.3, a CTZA with a methoxy-terminated alkyl linker chain of three methylene units at the C-6 position, exhibited the brightest emission, which produced 16.6-fold higher luminescence when combined with HSA (i.e. BBlue2.3/HSA pair) compared to that of the CTZ/HSA pair (**Figure 3**).

Based on these results, we predicted that elimination of the benzyl group at the C-8 position of BBlue2.3 would relieve its steric hindrance with key amino acids in the substrate binding site of HSA and enhance the enzymatic luminescence reaction of HSA. We then designed and synthesized a novel CTZA, named as Human Lumiphore 1 (HuLumino1) based on the synthetic procedures of BBlue2.3 [15] and an array of 5 CTZAs containing known analogues [20] to investigate the effect of substitution at the C-2, C-6, and C-8 positions of CTZ on serum albumin-dependent luminescence (**Figure 4b-d**). Moreover, the luminescence of

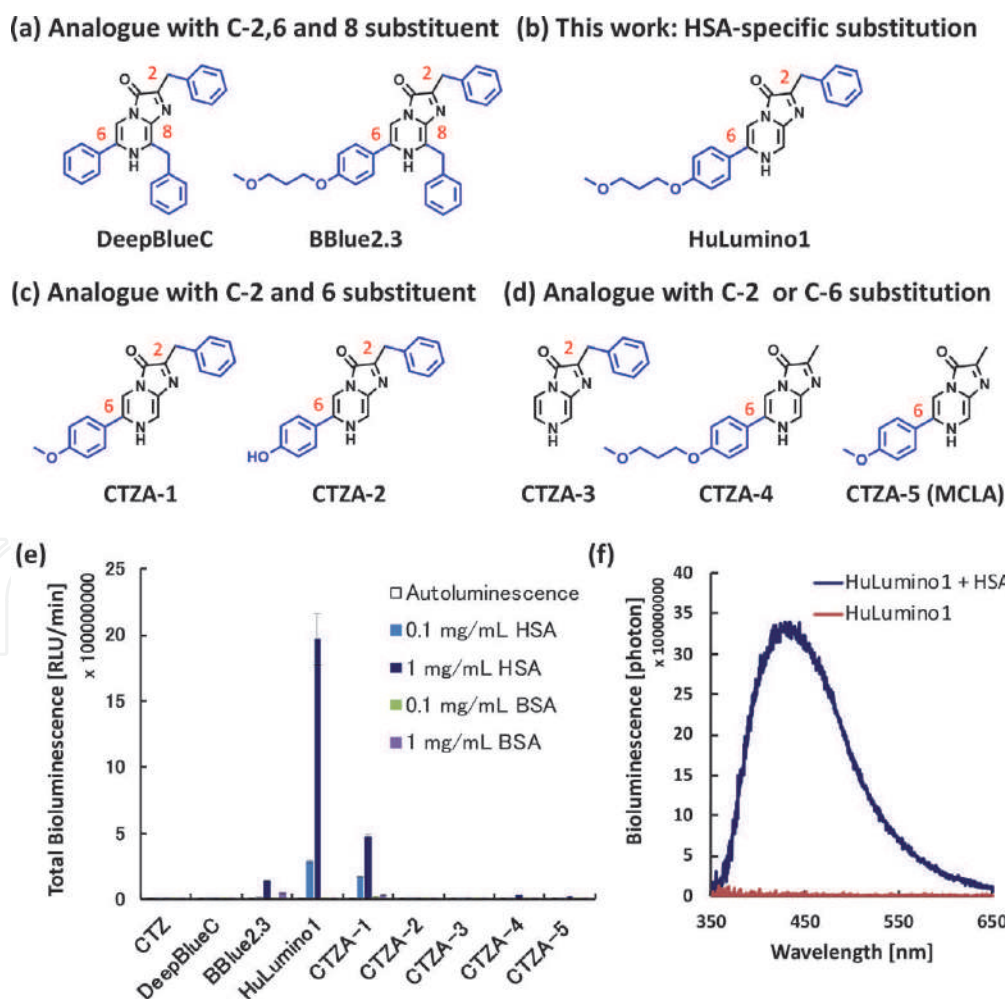


**Figure 4.** Chemical structures of coelenterazine analogues (CTZAs) upon (a) C-2, C-6, and C-8 substitutions, (b) HSA-specific substitution, (c) C-2 and C-6 substitution, and (d) C-2 or C-6 substitution. (e) Luminescence from serum albumins (0.1 or 1 mg/mL) treated with the indicated substrate (10  $\mu$ M); error bars represent the standard deviations of three measurements. (f) Bioluminescence spectra of HuLumino1 in the presence or absence of HSA.

commercially available CTZAs (DeepBlueC and MCLA) was compared with the synthesized CTZAs when fatty acid free HSA and BSA were added (**Figure 4e**). Although the autoluminescence levels in PB buffer of HuLumino1 was similar to that of CTZ, only HuLumino1 displayed significantly enhanced luminescence dependent on HSA (but not BSA containing fatty acid) concentrations, as indicated by the 14.1-fold higher emission compared with that of the BBlue2.3/HSA pair. Furthermore, the luminescence intensity of the HuLumino1/HSA pair was found to be 718-fold higher than that of the CTZ/BSA pair, which has been reported to produce luminescence [11, 12]. The HuLumino1/HSA pair exhibited flash-type luminescence with a peak wavelength of 432 nm. (**Figure 4f**). Unexpectedly, HuLumino1 selectively activated HSA by recognizing the subtle conformational difference in the substrate binding site, although the overall sequence homology between HSA and BSA is 75.6%.

These results suggest “luciferase” activity of HSA catalyzes the enzymatic luminescence reaction of CTZAs to produce “bioluminescence”.

## 2.2 Quantitative evaluation of luminescence intensity

To characterize the enzymatic luminescence reaction with HSA, the bioluminescence intensity of CTZAs and HSA pairs was quantitatively evaluated. Bioluminescence intensity is generally determined by several reaction factors including the bioluminescence quantum yield ( $\phi_{BL}$ ) of luciferin, turnover number ( $k_{cat}$ ), and active luciferase concentration. Kinetic parameters were determined using a custom-built luminometer with a photomultiplier tube (PMT) (H11890-01; Hamamatsu Photonics, Japan), and its absolute responsibility for total number of emitted photons in the instrument was calibrated for luminescence spectrum of each luciferin-luciferase pair [21, 22]. The absolute responsibility of the luminometer for the CTZ-utilizing bioluminescent system was determined as described previously [21]. The  $\phi_{BL}$  values were calculated from the total number of emitted photons and total number of reacted luciferin molecules. To integrate all photons derived from the enzymatic reaction, the number of photons was monitored using the luminometer from before initiating the reaction to until the reaction was completed. The reaction was initiating by injection of fatty acid-free HSA PB solution (100  $\mu\text{g}/\text{mL}$  or 10  $\text{mg}/\text{mL}$ ) into the preinstalled luciferin PB solution (20 nM) in the luminometer.

The Michaelis–Menten constant ( $K_m$ ) of luciferin was calculated from Lineweaver-Burk plots constructed using a standard method. The catalytic constant ( $k_{cat}$ ), which is the turnover number of the reaction for luciferin by a single luciferase molecule per second, was calculated from the  $\phi_{BL}$  value and maximum velocity ( $V_{max}$ ) determined from the Lineweaver-Burk plots.

The apparent  $K_m$  of the HuLumino1/HSA pair was 4.3  $\mu\text{M}$ , which was comparable to that of the NanoLuc system [23]. In contrast, the  $k_{cat}$  value of the NanoLuc system was 294-fold higher than that of the HuLumino1/HSA pair, and the catalytic efficiency of the luminescence reaction by HSA was lower than that of conventional luciferase [24]. However, in the luminescence system with HSA, HuLumino1 displayed a slightly higher  $K_m$  value than CTZA-1, but its  $k_{cat}$  value was approximately 3-fold higher (**Table 1**), resulting in 4.2-fold stronger light emission than that of CTZA-1 (**Figure 4e**). For luciferin with high enzyme affinity (e.g., CTZA-1), oxyluciferin, a product of the BL reaction, appears to competitively inhibit the luminescence reaction [25]. Moreover, HuLumino1 showed an enzyme affinity and bioluminescence quantum yield ( $\phi_{BL}$ ) of more than 5- and 100-fold higher than those of CTZ, respectively. The detailed luminescent profiles suggest that the structural properties of the alkyl linker chain modified at the C-6 position of the

Pair	$\varphi_{BL}^a [\times 10^{-5}]$	$K_m^b [\mu M]$	$k_{cat}^c [s^{-1}]$
CTZ/HSA	$0.32 \pm 0.03$	$25.3 \pm 5.2$	$2.75 \pm 0.3$
HuLumino1/HSA	$30.9 \pm 3.1$	$4.28 \pm 1.24$	$0.30 \pm 0.06$
CTZA-4/HSA	$42.2 \pm 9.1$	$2.46 \pm 0.40$	$0.11 \pm 0.09$

<sup>a-c</sup>Errors represent standard error of the mean values for triplicate experiments.

<sup>b</sup>Michaelis-Menten constant ( $K_m$ ) values were determined by Lineweaver-Burk plots via measurements of initial rates of light emission over a range 0.5 to 20  $\mu M$ .

<sup>c</sup>Turnover rate ( $k_{cat}$ ) values were calculated by dividing maximum velocity ( $V_{max}$ ) by the  $\varphi_{BL}$ . The  $V_{max}$  were determined by Lineweaver-Burk plots.

**Table 1.**  
Luminescent profiles of CTZ and its analogues with HSA.

imidazopyrazinone core contribute to the efficient HSA-catalyzed emission reaction. Although the catalytic efficiency of HuLumino1/HSA is much lower than that of the NanoLuc system, HuLumino1 is a luciferin that is relatively more suitable for HSA than other existing luminescent substrates.

### 2.3 Enzymatic reaction site of HSA

The crystal structure of HSA, with binding to a variety of drugs, clarified the two principal drug binding sites in different subdomains (site 1 in subdomain IIA and site 2 in subdomain IIIA) [26, 27]. To investigate the luminescent reaction site between HSA and HuLumino1, a competitive assay was conducted with two site-specific HSA drugs (warfarin-site1 and ibuprofen-site2) [27]. Fatty acid free HSA PB solution was pre-treated with the drugs (0–100  $\mu M$ ) to fill binding site 1 or 2 before adding HuLumino1. The luminescence of HuLumino1 was negligibly low in the presence of HSA-ibuprofen complex (**Figure 5a**). In contrast, HuLumino1 exhibited efficient luminescence with the HSA-warfarin complex, indicating that HuLumino1 selectivity binds to the site 2 cavity of HSA. In detailed analysis of the inhibitory kinetics, Lineweaver-Burk plots displayed that ibuprofen competitively inhibited the binding of HuLumino1 to HSA ( $K_i$  of ibuprofen was 6.3 nM) (**Figure 5b**). Therefore, the enzymatic reaction site of HuLumino1 was experimentally determined to be binding site 2. Next, docking simulation with the Molecular Operating Environment software package was carried out to predict the binding poses. The simulation displayed the specific binding of HuLumino1 to the hydrophobic cavity of site 2 by interacting with several amino acids including R410, K414, and L453 (**Figure 5c–e**). Particularly, R410, a key amino acid residue in the esterase activity of HSA [17], is also involved in the luminescence reaction (**Figure 5e**).

Next, to investigate the effect of the steric structure of HSA on luminescence, HSA pretreated with 10 M guanidine hydrochloride, a reagent commonly used to induce denaturation of the  $\alpha$ -helix structure of proteins [28], was prepared, and the luminescence of HuLumino1 was extremely low in the presence of denatured HSA (data not shown). Therefore, the enzymatic reaction of HuLumino 1 depends on the microenvironment and steric structure such as binding site 2 constructed by the folding structure of HSA. These results suggest that emission of HuLumino1/HSA is not a non-specific chemiluminescence commonly found in other imidazopyrazinone compounds.

### 2.4 Bioluminescent assay for HSA

Low levels of HSA in the serum (<35 mg/mL) are biomarkers of several diseases such as malnutrition, cirrhosis, and chronic hepatitis [29]. In hospitals, HSA is

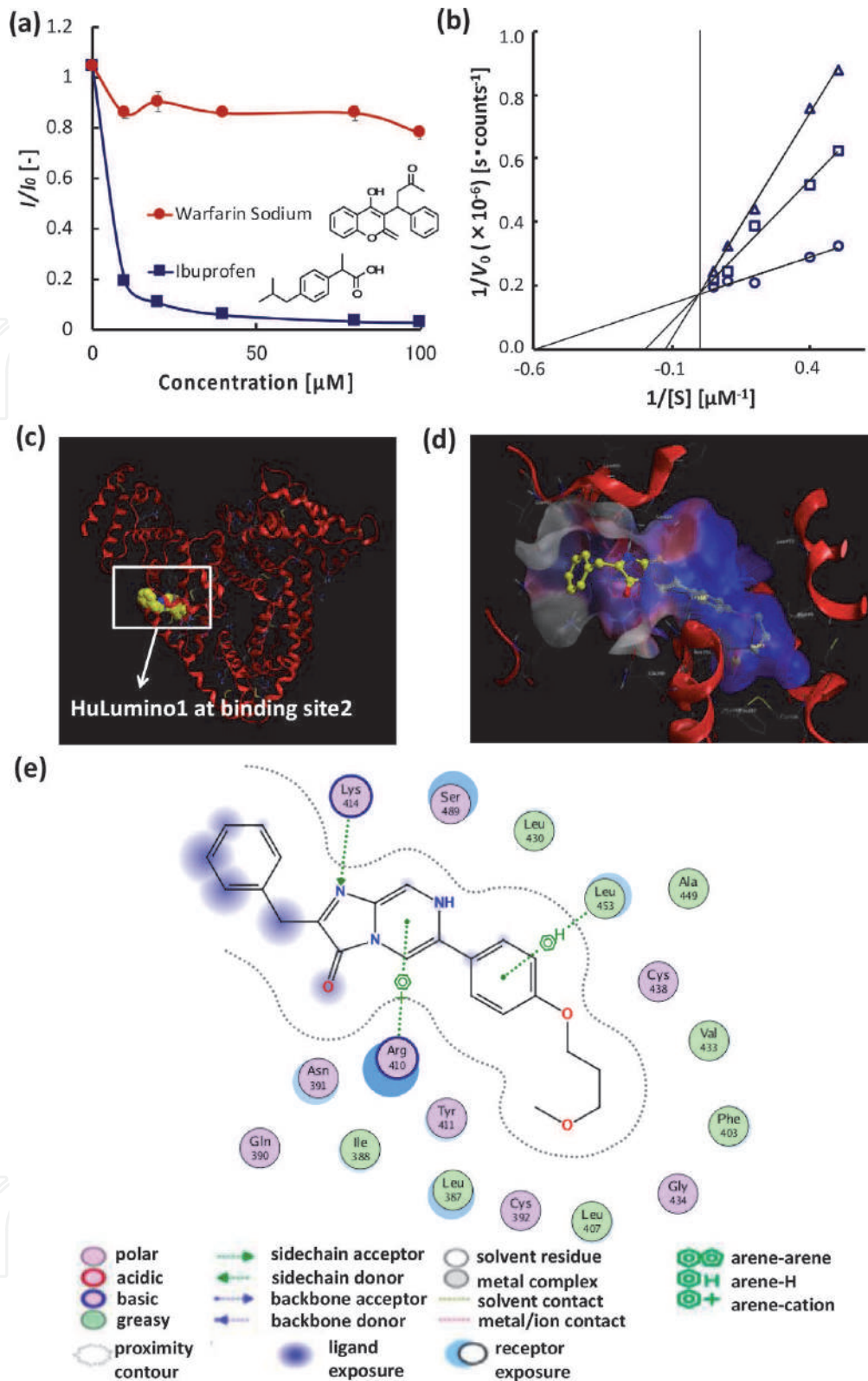


**Figure 5.** (a) Luminescence response in the presence ( $I$ ) vs. absence ( $I_0$ ) of the binding drug concentration (0–100  $\mu\text{M}$ ). (b) Lineweaver-Burk plot indicating competitive inhibition by ibuprofen.  $V_0$  is defined as the luminescence intensity over the initial 30 s and  $[S]$  is the substrate concentration. The concentrations of ibuprofen were 1 nM (square) and 5 nM (triangle). Open circles indicate negative controls with no ibuprofen. (c) Ligand-binding site 2 of HSA with HuLumino1 as posed by the molecular operating environment software (d) magnified view of binding site 2. The ligand binding site in the blue region indicates the presence of the hydrophobic environment. (e) Predicted interaction between HuLumino1 and HSA.

evaluated using the colorimetric bromocresol green assay or ELISA. Both can provide a reliable assessment of albumin but require sample preparation and processing time (e.g. 3 h for ELISA) [30]. Therefore, an assay for the simple, accurate and

rapid detection of HSA in the serum should be developed for clinical diagnosis. We demonstrated that the BL assay can be used to evaluate HSA based on the enzymatic luminescence reaction of HuLumino1. Regarding the selectivity of the reaction of HuLumino1, no reactivity with other proteins (BSA,  $\beta$ -galactosidase,  $\beta$ -lactoglobulin, catalase,  $\alpha$ -chymotrypsinogen, hemoglobin, human IgG, porcine lipase, papain, pepsin, trypsin,  $\gamma$ -globulin, carbonic anhydrase, concanavalin A, glucosidase, histone, myoglobin, and RNase, 0.1 mg/mL) was observed, and only HSA led to distinct luminescence enhancement (**Figure 6a**). Although the coexistence of most proteins did not affect the enzymatic reaction of the HSA/HuLumino1 pair, a slight decrease in luminescence was observed in the presence of some proteins (data not shown). This indicates that HuLumino1 nonspecifically binds to other proteins but does not exhibit BL. Hence, HuLumino1 can be used to detect HSA without interference from other proteins, as it exhibited excellent selectivity for HSA even in a complicated biological system. The luminescence of HuLumino1 was enhanced in an HSA concentration-dependent manner and exhibited a constant intensity at HSA concentrations above 10 mg/mL (**Figure 6b**). A linear increase in luminescence, within the spiked HSA concentration range of 0–0.1 mg/mL in PBS-diluted serum, resulted in a detection limit of 8.6  $\mu$ g/mL for HSA, which was comparable to the standard detection limit of HSA in physiological systems (**Figure 6c**) [31].

Finally, two HSA assays, including our developed BL-based assay and ELISA, were performed to evaluate human serum from male AB plasma. The HSA levels calculated with HuLumino1 agreed well with those estimated by ELISA within 5% error. The spike and recovery tests also showed results within the margin of 7%

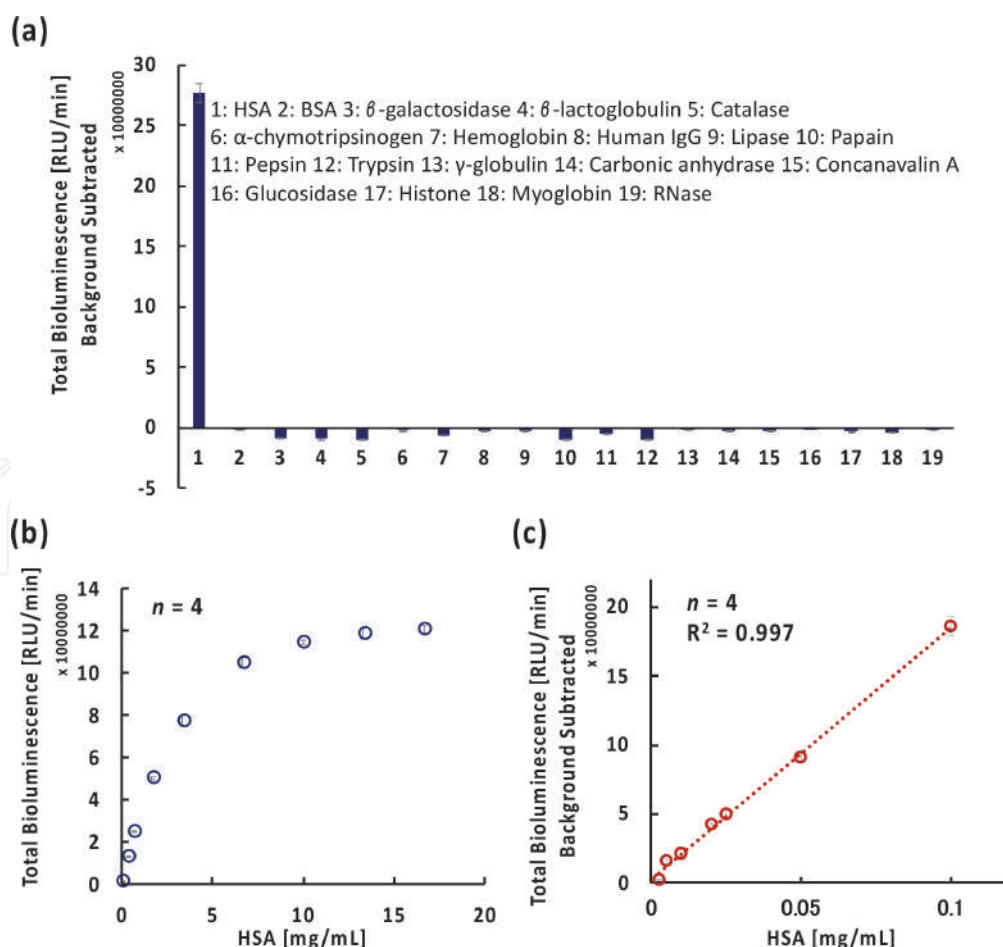


**Figure 6.** (a) Variation in luminescence of HuLumino1 (10  $\mu$ M) in the presence of proteins (0.1 mg/mL); error bars represent the standard deviations of three measurements. (b) Luminescence intensity of HuLumino1 (20  $\mu$ M) containing various concentrations of HSA (0–17 mg/mL) in PBS and (c) HSA (0–17 mg/mL) in PBS-diluted plasma (100-fold, pH 7.4).

Amount of HSA added (mg/mL)	HSA (mg/mL) determined by developed method <sup>a</sup>	HSA (mg/mL) determined by ELISA	Recovery
0	39.0 ± 3.1	41.0 ± 3.6	95.2
1	44.5 ± 0.5	ND	106.1
2.5	45.2 ± 0.5	ND	104.1

ND: Not Determined.

<sup>a</sup>Conditions: HuLumino1 (20 μM) in PBS-diluted serum (1000-fold, 10 mM, pH 7.4).

**Table 2.**  
Assay of HSA in human serum.

error (Table 2). Therefore, the BL-based HSA assay showed analytical capability with high sensitivity and could detect HSA within 10 min including the sample preparation and measurement times. In addition, we detected the expression of recombinant HSA in living COS-1 cells (data not shown), indicating that HuLumino1 can be used in molecular biology studies and in biomedical applications.

We designed and synthesized the first luciferin (HuLumino1), an analogue with C-6 and C-8 modification of CTZ, which exhibited bioluminescence with HSA. HuLumino1 rapidly detected HSA with high sensitivity and specificity, even in real human plasma containing various interfering biomolecules. Detailed kinetic investigation of the enzymatic reaction clarified the enzyme recognition of HuLumino1 from HSA drug binding site 2, resulting a highly selective reaction and revealing a reaction with both native HSA and recombinant HSA expressed in COS-1 cells. Therefore, the BL-based assay with HuLumino1, either used alone or coupled with ELISA, can be used for the early diagnosis of HSA-related diseases, enabling accurate and rapid detection of HSA in serum samples without pre-treatment. The information obtained through detailed investigation of the HuLumino1/HSA pair may be extended to protein assays based on a luminescent reaction without genetically engineered luciferases.

## Acknowledgements

We acknowledge funding from JST, PRESTO Grant Number JPMJPR20EB, JSPS KAKENHI Grant Number 20 K15421, AMED under Grant Number JP191m0203012, Shimazu Science Foundation, Research Foundation for Opto-Science and Technology, and Nakatani Foundation for Advancement of Measuring Technologies in Biomedical Engineering, and DAICENTER project grant from DBT (Govt. of India) to Renu Wadhwa and special strategic grant from AIST (Japan).

## Conflict of interest

The authors declare no conflict of interest.

## Notes/thanks/other declarations

We thank Dr. Tsukasa Ishihara (Biomedical Research Institute, National Institute of Advanced Industrial International Science and Technology) for his help with the docking simulation experiment.

IntechOpen

### **Author details**

Ryo Nishihara<sup>1\*</sup>, Kazuki Niwa<sup>1</sup>, Tatsunosuke Tomita<sup>1</sup> and Ryoji Kurita<sup>1,2</sup>

1 National Institute of Advanced Industrial Science and Technology (AIST),  
Tsukuba, Japan

2 University of Tsukuba, Tsukuba, Japan

\*Address all correspondence to: r.nishihara@aist.go.jp

### **IntechOpen**

---

© 2021 The Author(s). Licensee IntechOpen. This chapter is distributed under the terms of the Creative Commons Attribution License (<http://creativecommons.org/licenses/by/3.0>), which permits unrestricted use, distribution, and reproduction in any medium, provided the original work is properly cited. 

## References

- [1] Shimomura O. *Bioluminescence: Chemical Principles and Methods*. Bioluminescence: Chemical Principles and Methods. Singapore: World Scientific Publishing Company; 2006. 471 p.
- [2] Badr C. *Bioluminescent Imaging: Methods and Protocols*. Bioluminescent Imaging: Methods and Protocols. New York: Springer; 2014. 1276 p.
- [3] Rowe L, Dikici E, Daunert S. Engineering bioluminescent proteins: expanding their analytical potential. *Analytical Chemistry*. 2009;81(21): 8662–8668. DOI: 10.1021/ac9007286
- [4] Ozawa T, Yoshimura H, Kim S. Advances in fluorescence and bioluminescence imaging. *Analytical Chemistry*. 2013;85(2):590–609. DOI: 10.1021/ac3031724
- [5] Mofford D, Reddy G, Miller S. Latent luciferase activity in the fruit fly revealed by a synthetic luciferin. *Proceedings of the National Academy of Sciences of the United States of America*. 2014;111(12):4443–4448. DOI: 10.1073/pnas.131900111
- [6] Mofford D, Liebmann K, Sankaran G, Reddy G, Reddy G, Miller S. Luciferase activity of insect fatty acyl-CoA synthetases with synthetic luciferins. *ACS Chemical Biology*. 2017;12(12):2946–2951. DOI: 10.1021/acdchembio.7b00813
- [7] Mofford D, Adams S, Reddy G, Reddy G, Miller S. Luciferin amides enable in vivo bioluminescence detection of endogenous fatty acid amide hydrolase activity. *Journal of the American Chemical Society*. 2015;137(27):8684–8687. DOI: 10.1021/jacs.5b04357
- [8] Liu R, Tang J, Xu Y, Dai Z. Bioluminescence imaging of inflammation in vivo based on bioluminescence and fluorescence resonance energy transfer using nanobubble ultrasound contrast agent. *ACS Nano*. 2019;13(5):5124–5132. DOI: 10.1021/acsnano.8b08359.
- [9] Gross S, Gammon S, Moss B, Rauch D, Harding J, Heinecke J, et al. Bioluminescence imaging of myeloperoxidase activity in vivo. *Nature Medicine*. 2009;15(4):455–461. DOI: 10.1038/nm.1886
- [10] Nishihara R, Niwa K, Tomita T, Kurita R. Coelenterazine analogue with human serum albumin-specific bioluminescence. *Bioconjugate Chemistry*. 2020;31(12):2679–2684. DOI: 10.1021/acs.bioconjchem.0c00536
- [11] Vassel N, Cox C, Naseem R, Morse V, Evans R, Power R, et al. Enzymatic activity of albumin shown by coelenterazine chemiluminescence. *Luminescence*. 2012;27(3):234–241. DOI: 10.1002/bio.2357
- [12] Lindberg E, Mizukami S, Iyata K, Miyawaki A, Kikuchi K. Development of luminescent coelenterazine derivatives activatable by beta-galactosidase for monitoring dual gene expression. *Chemistry-A European Journal*. 2013;19(44):14970–14976. DOI: 10.1002/chem.201302002
- [13] Maguire C, Bovenberg M, Crommentuijn M, Niers J, Kerami M, Teng J, et al. Triple bioluminescence imaging for in vivo monitoring of cellular processes. *Molecular Therapy-Nucleic Acids*. 2013;2(6):e99. DOI: 10.1038/mtna.2013.25
- [14] Hall M, Unch J, Binkowski B, Valley M, Butler B, Wood M, et al. Engineered luciferase reporter from a deep sea shrimp utilizing a novel imidazopyrazinone substrate. *ACS*

Chemical Biology. 2012;7(11):1848–1857. DOI: 10.1021/cb3002478

[15] Nishihara R, Paulmurugan R, Nakajima T, Yamamoto E, Natarajan A, Afjei R, et al. Highly bright and stable NIR-BRET with blue-shifted coelenterazine derivatives for deep-tissue imaging of molecular events in vivo. *Theranostics*. 2019;9(9):2646–2661. DOI: 10.7150/thno.32219

[16] Anderson N, Anderson N. The human plasma proteome: history, character, and diagnostic prospects. *Molecular & Cellular Proteomics*. 2002; 1(11):845–867. DOI: 10.1074/mcp.r200007-mcp200

[17] Kragh-Hansen U. Molecular and practical aspects of the enzymatic properties of human serum albumin and of albumin-ligand complexes. *Biochimica Et Biophysica Acta-General Subjects*. 2013;1830(12):5535–5544. DOI: 10.1016/j.bbagen.2013.03.015

[18] Taverna M, Marie A, Mira J, Guidet B. Specific antioxidant properties of human serum albumin. *Annals of Intensive Care*. 2013;3(1):4. DOI: 10.1186/2110-5820-3-4

[19] Hollfelder F, Kirby A, Tawfik D, Kikuchi K, Hilvert D. Characterization of proton-transfer catalysis by serum albumins. *Journal of the American Chemical Society*. 2000;122(6):1022–1029. DOI: 10.1021/ja993471y

[20] Hirano T, Gomi Y, Takahashi T, Kitahara K, Qi C, Mizoguchi I, et al. Chemiluminescence of coelenterazine analogs - structures of emitting species. *Tetrahedron Letters*. 1992;33(39):5771–5774. DOI: 10.1016/0040-4039(92)89028-B

[21] Ikeda Y, Tanaka M, Nishihara R, Hiruta Y, Citterio D, Suzuki K, et al. Quantitative evaluation of luminescence intensity from enzymatic luminescence reaction of coelenterazine and

analogues. *Journal of Photochemistry and Photobiology A Chemistry*. 2020: 112459. DOI: 10.1016/j.jphotochem.2020.112459

[22] Ando Y, Niwa K, Yamada N, Enomoto T, Irie T, Kubota H, et al. Firefly bioluminescence quantum yield and colour change by pH-sensitive green emission. *Nature Photonics*. 2008; 2(1):44–47. DOI: 10.1038/nphoton.2007.251

[23] Coutant E, Gagnot G, Hervin V, Baatallah R, Goyard S, Jacob Y, et al. Bioluminescence profiling of NanoKAZ/ NanoLuc luciferase using a chemical library of coelenterazine analogues. *Chemistry-A European Journal*. 2020;26 (4):948–958. DOI: 10.1002/chem.201904844

[24] Yeh H, Karmach O, Ji A, Carter D, Martins-Green M, Ai H. Red-shifted luciferase-luciferin pairs for enhanced bioluminescence imaging. *Nature Methods*. 2017;14(10):971–974. DOI: 10.1038/nmeth.4400

[25] Matthews JC, Hori K, Cormier MJ. Substrate and substrate analog binding properties of Renilla luciferase. *Biochemistry*. 1977;16(24):5217–5220. DOI: 10.1021/bi00643a009

[26] Sugio S, Kashima A, Mochizuki S, Noda M, Kobayashi K. Crystal structure of human serum albumin at 2.5 Å resolution. *Protein Engineering*. 1999;12 (6):439–446. DOI: 10.1093/protein/12.6.439

[27] Ghuman J, Zunszain P, Petitpas I, Bhattacharya A, Otagiri M, Curry S. Structural basis of the drug-binding specificity of human serum albumin. *Journal of Molecular Biology*. 2005;353 (1):38–52. DOI: 10.1016/j.jmb.2005.07.075

[28] Xu Y, Su M, Li H, Liu Q, Xu C, Yang Y, et al. A fluorescent sensor for discrimination of HSA from BSA

through selectivity evolution. *Analytica Chimica Acta*. 2018;1043:123–131. DOI: 10.1016/j.aca.2018.09.010

[29] Murch S, Winyard P, Koletzko S, Wehner B, Cheema H, Risdon R, et al. Congenital enterocyte heparan sulphate deficiency with massive albumin loss, secretory diarrhoea, and malnutrition. *Lancet*. 1996;347(9011):1299–1301. DOI: 10.1016/s0140-6736(96)90941-1

[30] Luo Z, Lv T, Zhu K, Li Y, Wang L, Gooding J, et al. Paper-based ratiometric fluorescence analytical devices towards point-of-care testing of human serum albumin. *Angewandte Chemie-International Edition*. 2020;59(8):3131–3136. DOI: 10.1002/anie.201915046

[31] Gao T, Yang S, Cao X, Dong J, Zhao N, Ge P, et al. Smart self-assembled organic nanoprobe for protein-specific detection: design, synthesis, application, and mechanism studies. *Analytical Chemistry*. 2017;89(18):10085–10093. DOI: 10.1021/acs.analchem.7b02923

# We are IntechOpen, the world's leading publisher of Open Access books Built by scientists, for scientists

6,300

Open access books available

171,000

International authors and editors

190M

Downloads

Our authors are among the

154

Countries delivered to

TOP 1%

most cited scientists

12.2%

Contributors from top 500 universities



WEB OF SCIENCE™

Selection of our books indexed in the Book Citation Index  
in Web of Science™ Core Collection (BKCI)

Interested in publishing with us?  
Contact [book.department@intechopen.com](mailto:book.department@intechopen.com)

Numbers displayed above are based on latest data collected.  
For more information visit [www.intechopen.com](http://www.intechopen.com)



# Near-Infrared Luciferin Analogs for *In Vivo* Optical Imaging

Ryohei Saito-Moriya, Rika Obata and Shojiro A. Maki

## Abstract

The firefly bioluminescence reaction has been exploited for *in vivo* optical imaging in life sciences. To develop highly sensitive bioluminescence imaging technology, many researchers have synthesized luciferin analogs and luciferase mutants. This chapter first discusses synthetic luciferin analogs and their structure–activity relationships at the luminescence wavelength of the firefly bioluminescence reaction. We then discuss the development of luciferin analogs that produce near-infrared (NIR) light. Since NIR light is highly permeable for biological tissues, NIR luciferin analogs might sensitively detect signals from deep biological tissues such as the brain and lungs. Finally, we introduce two NIR luciferin analogs (TokeOni and seMpai) and a newly developed bioluminescence imaging system (AkaBLI). TokeOni can detect single-cell signals in mouse tissue and luminescence signals from marmoset brain, whereas seMpai can detect breast cancer micro-metastasis. Both reagents are valid for *in vivo* bioluminescence imaging with high sensitivity.

**Keywords:** Firefly bioluminescence, Bioluminescence imaging, Structure–activity relationships, Multicolor, Near-infrared light

## 1. Introduction

In Japan, watching the light of fireflies has been a summer tradition for over one thousand years. Modern fireflies are known to glow yellow-green, but in ancient times they emitted a dark green luminescence, as confirmed by recent molecular biology techniques [1]. The detailed mechanism of firefly bioluminescence is described in previous chapters. This chapter focuses on synthetic substrates of firefly luciferase, which are employed in firefly bioluminescence imaging (BLI).

In recent biological research, BLI technology has observed biological events *in vivo* [2–8]. For example, in cancer research, BLI has been applied to real-time monitoring of gene expression, cell numbers, and other biological events in transgenic mouse models [9–16]. Our group has developed firefly substrate analogs for use in these research fields.

The firefly bioluminescence reaction proceeds via the oxidation of *D*-luciferin (**1**, LH2, **Figure 1**) catalyzed by firefly luciferase (Fluc) in the presence of adenosine triphosphate (ATP),  $Mg^{2+}$  and  $O_2$  by a two-step reaction. In the first step, LH2 is adenylated with ATP, and is then oxidized by  $O_2$ , forming excited-state oxyluciferin that relaxes to the ground state with yellow-green light emission ( $\lambda_{max} = 560$  nm) [17–19]. However, yellow-green light is not able to easily penetrate biological tissues [20], and is useful only for imaging shallow tissues such as subcutaneous tissues. To detect signals from deep tissues such as brain and lung [21], near-infrared (NIR)

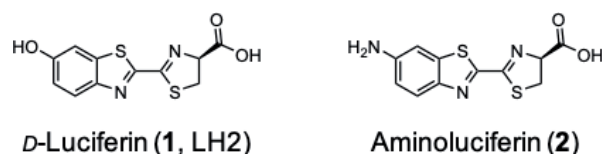


**Figure 1.**  
Structures of *D*-luciferin (**1**, LH2) and aminoluciferin (**2**).

light should be used, as it is highly permeable to biological tissues [20] and is suitable for *in vivo* deep tissue imaging [21]. Recently, many synthetic luciferin analogs have been reported. Our group has synthesized various luciferin analogs and compared them with **1**. By studying the structure–activity relationships of these analogs and *Photinus pyralis* (*Ppy*) luciferase, we have developed luciferin analogs that produce wide-spectrum light (from blue to red), along with NIR luciferin analogs (AkaLumine, TokeOni, seMpai) for BLI. Our different analogs are described in this chapter.

## 2. Luciferin analogs of firefly luciferase

Many researchers have synthesized luciferin analogs, and different substrates reacted with luciferases exhibit different luminescence activities [22–24]. Most luciferin analogs are formed by modifying the benzothiazole moiety of **1**. Analogs of **1** were first synthesized by White *et al.* in 1966. They showed that aminoluciferin (**2**, **Figure 1**), in which the hydroxyl group of benzothiazole is replaced with an amino group, can function as a substrate of Fluc and emit red bioluminescence [25].

### 2.1 Development of luciferin analogs based on LH2

As mentioned above, many luciferin analogs are prepared by modifying the benzothiazole moiety of **1** [22–24]. For instance, *N*-cycloaminoluciferins (**2a–f**, **Figure 2A**) are prepared by cyclizing the NH<sub>2</sub> of **2**. These analogs were reported by two independent groups, who synthesized them by different routes [26, 27] (**Figure 2B–C**). When reacted with Fluc, **2a–f** show longer wavelengths than **1**, probably reflecting the electron donation effect of cycloamine substitutes. Comparing the bioluminescence activities and emission wavelengths of analogs **2e** and **2f** on Fluc and Fluc mutant luciferase R218K, it was found that **2e**/Fluc and **2f**/R218K produced light at 604 and 614 nm, respectively, whereas **2e**/R218K and **2f**/Fluc produced no light [26]. The interaction between the active site of luciferase and the substrate is very critical, indicating that the structures of both reactants play essential controlling roles in luminescence activity.

Miller *et al.* synthesized CycLuc1 (**7a**, **Figure 3**) by fusing *N*-cycloalkylation of **2** with benzothiazole [28]. Analog **7a** exhibited a longer luminescence wavelength on Fluc (599 nm) than **1** on Fluc, and was emitted more intensely than **1** in a *Photuris pennsylvanica* firefly luciferase mutant (Ultra-Glo). The BLI of **7a** detects the signals from deep organs such as brains and lungs [21, 29]. Li *et al.* synthesized CybLuc (**7b**, **Figure 3**) by substituting the hydroxy group of **2** with a cycloamino group. Analog **7b** produced light at 603 nm and its BLI detected the signals from mouse brain [30].

Iwano *et al.* developed luciferin analogs **8a–g** (**Figure 4A**) by substituting the benzothiazole moiety of **1** with a simple benzene ring and extended  $\pi$ -conjugations [31]. Olefins were extended by the Wittig reaction from **10c–d** and **12e–f** as starting

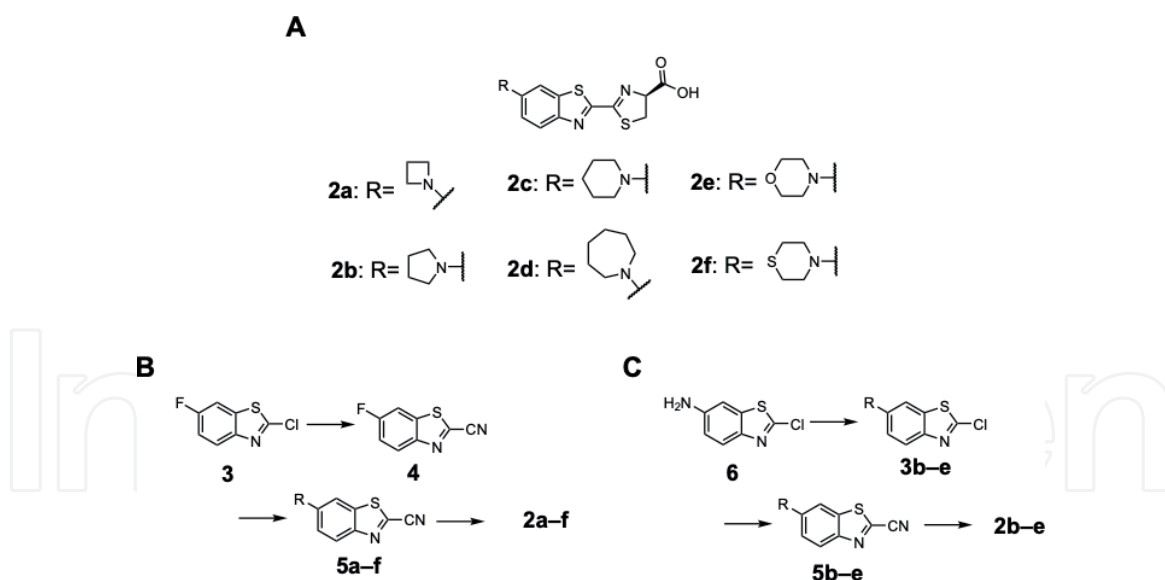


**Figure 2.** Structures and synthetic routes of luciferin analogs **2a–f**. (A) *N*-cycloaminoluciferin analogs **2a–f**, (B) the synthetic route reported by Miller *et al.* [28], and (C) the synthetic route reported by Hirano *et al.* [29].

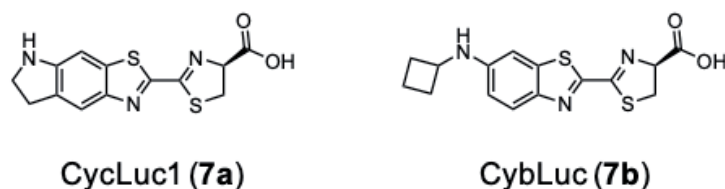


**Figure 3.** Structures of CycLuc1 (**7a**) and CybLuc (**7b**).

materials. In this synthesis, hydrolysis was stepwise followed by condensation with *D*-Cys(STrt)-OMe, thiazoline cyclization, and methyl ester deprotection (**Figure 4B**). The obtained analogs **8a–f** produced luminescent colors over a wide range (blue to red) [31]. Among these, AkaLumine (**8e**), which produces light at 675 nm, is a leading compound for NIR luciferin analogs, as described in Section 2.2. Later, analog **8e** was used as a reagent for BLI. In the same paper, 3-hydroxyl analog **8g** (**Figure 4A**) was also synthesized, but this analog produced no light [31]. Therefore, the position of the OH substituent is critical in the firefly bioluminescence reaction.

In contrast, the thiazoline site is rarely modified. Conley *et al.* synthesized a seleno-aminoluciferin analog **13a** (**Figure 5A**) in which the S of the thiazoline ring of **2** was replaced with Se [32], and Ioka *et al.* synthesized O- or C- substituted analogs **13b–c** (**Figure 5A**) [33]. Analog **13a**, which produced light at 600 nm, was synthesized by the cyclization reaction of selenocysteine (**Figure 5B**) [32]. Analog **13b** was obtained by synthesizing an amide **16b** synthesizing an amide from *D*-serine, cyclizing it with diethylaminosulfur trifluoride (DAST), and hydrolyzing it with Amano lipase (**Figure 5C**). Analog **13c** was prepared by coupling with bromothiazole **19** and pyrrolidione carboxylate **21** to form glutamate-linked benzothiazole **16c**, and cyclizing **16c** with trifluoroacetic acid (TFA) (**Figure 5D**). Interestingly, **13c** produces light at 547 nm, whereas **13b** is non-bioluminescence [33] but shows chemiluminescent ability. This result indicates that the thiazoline of **1** is an essential moiety for recognizing the activity site in luciferase.

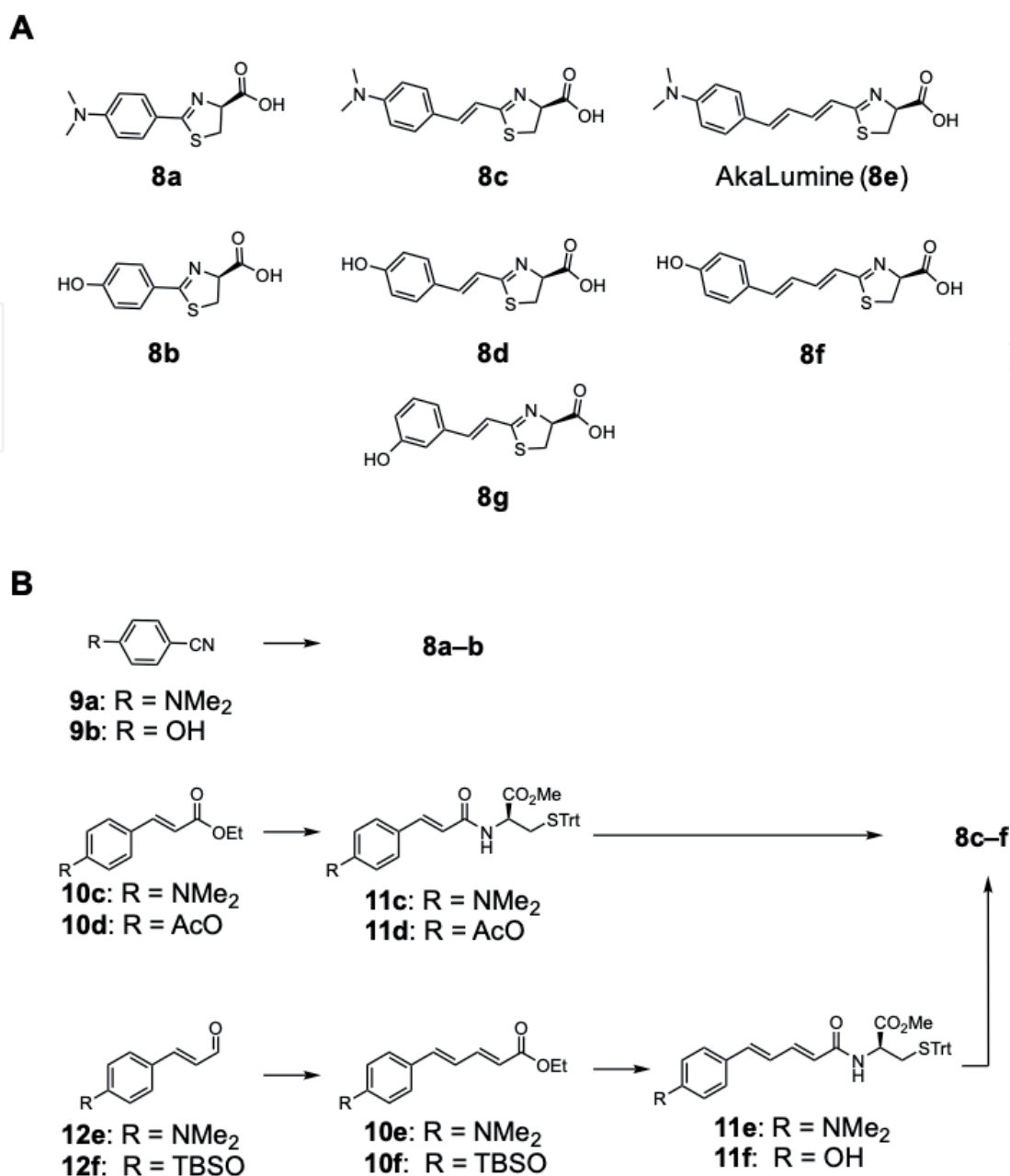


**Figure 4.**  
Structures of **8a–g** (A) and their synthetic routes **8a–f** (B).

## 2.2 Structure–activity relationships for developing NIR luciferin analogs

Based on these structure–activity relationships, additional luciferin analogs have been designed and synthesized for NIR light production. For example, Anderson *et al.* synthesized iLH2 (**22**, **Figure 6**) by inserting an olefin into the structure of **1**. Analog **22** produced NIR light at 706 nm [34]. However, the luciferase used at that time was a mutant (S284T), and the luminescence wavelength on Fluc was 670 nm. The same authors developed an *in vivo* dual-imaging technique that combines **1** and **22** with two different luciferases. This system can potentially observe new biological events by tracking two processes simultaneously [35]. Hall *et al.* synthesized NH<sub>2</sub>–NpLH2 (**23**, **Figure 6**) by extended conjugation of **2**. Analog **23** produced no light with Fluc, but its luminescence wavelength was extended to 743 nm by reaction with CBR2, a mutant luciferase of click beetles (*Pyrophorus plagiophthalmus*) [36]. All of these studies achieved long-wavelength emissions from mutant luciferases, but their luminescence activity is much lower than that of combinations of **1** and wild type *Ppy* luciferase.

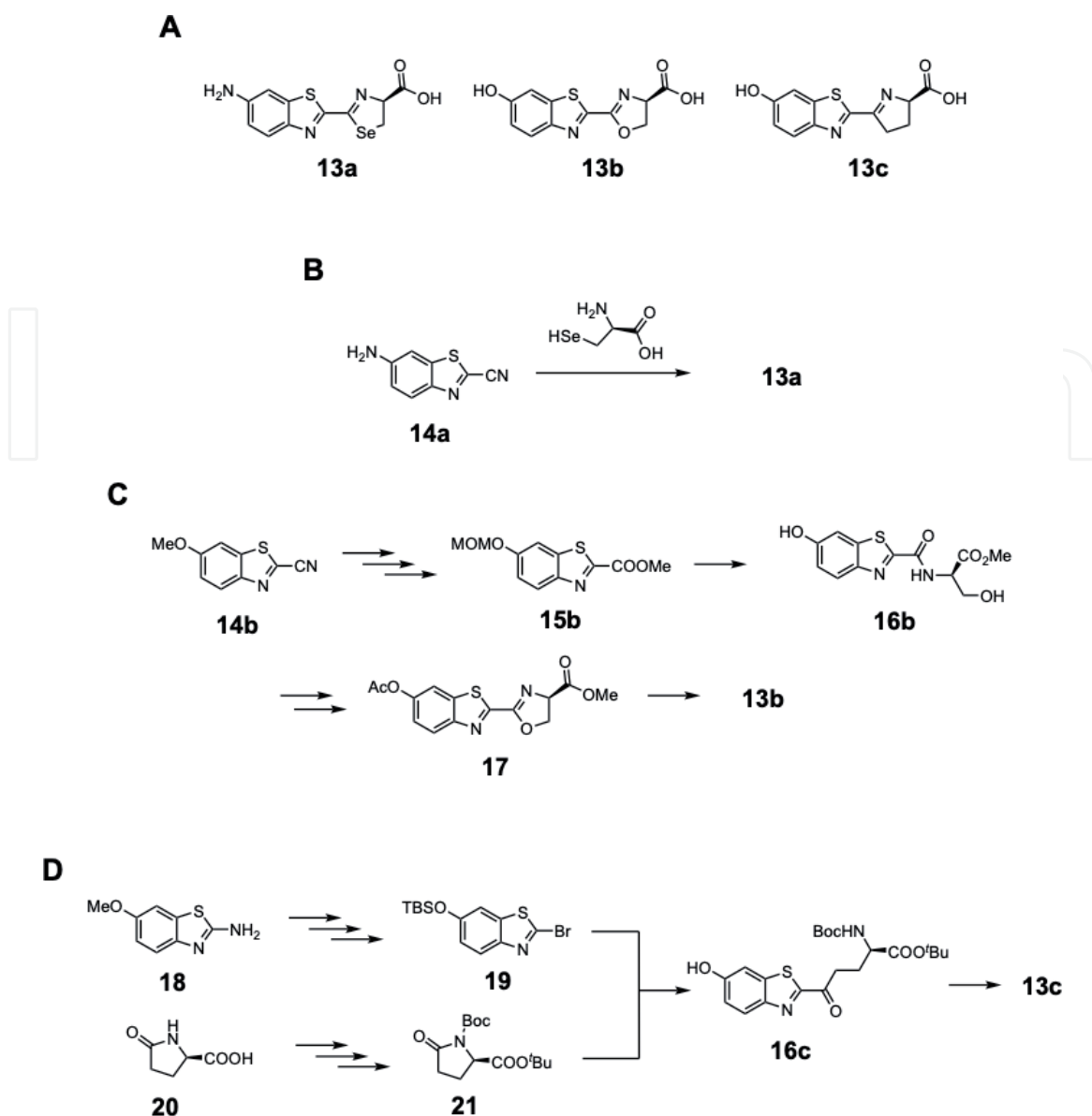


**Figure 5.** Structures of **13a–c** (A) and their synthetic routes **13a** (B), **13b** (C) and **13c** (D).

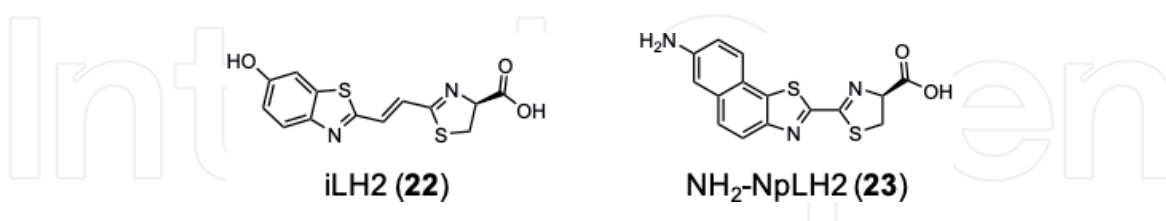


**Figure 6.** Structures of NIR luciferin analogs **iLH2** (22) and **NH<sub>2</sub>-NpLH2** (23).

Meanwhile, Maki's group has developed a number of analogs based on the structure of **8e**, which are expected to produce NIR light. Miura *et al.* formed a mother skeleton by a coupling reaction, and thus synthesized biphenyl analogs **24a–c** (Figure 7 and 8A) [37]. Analog **24a** produced light at 675 nm, but the luminescence intensity was weak. Although its conjugation was more extended than in **8e**, the luminescence wavelength of **24a** did not change as that of **8e** (675 nm). This result suggests that the biphenyl moiety rotates and reduces the fluorescent intensity.

Kiyama *et al.* synthesized cyclic amino analogs of **8e** (**25a–d**, Figure 7) [38] from 4-fluorobenzaldehyde **32** as the starting material. They replaced the F group with various secondary amines, and conducted the Horner–Wadsworth–Emmons

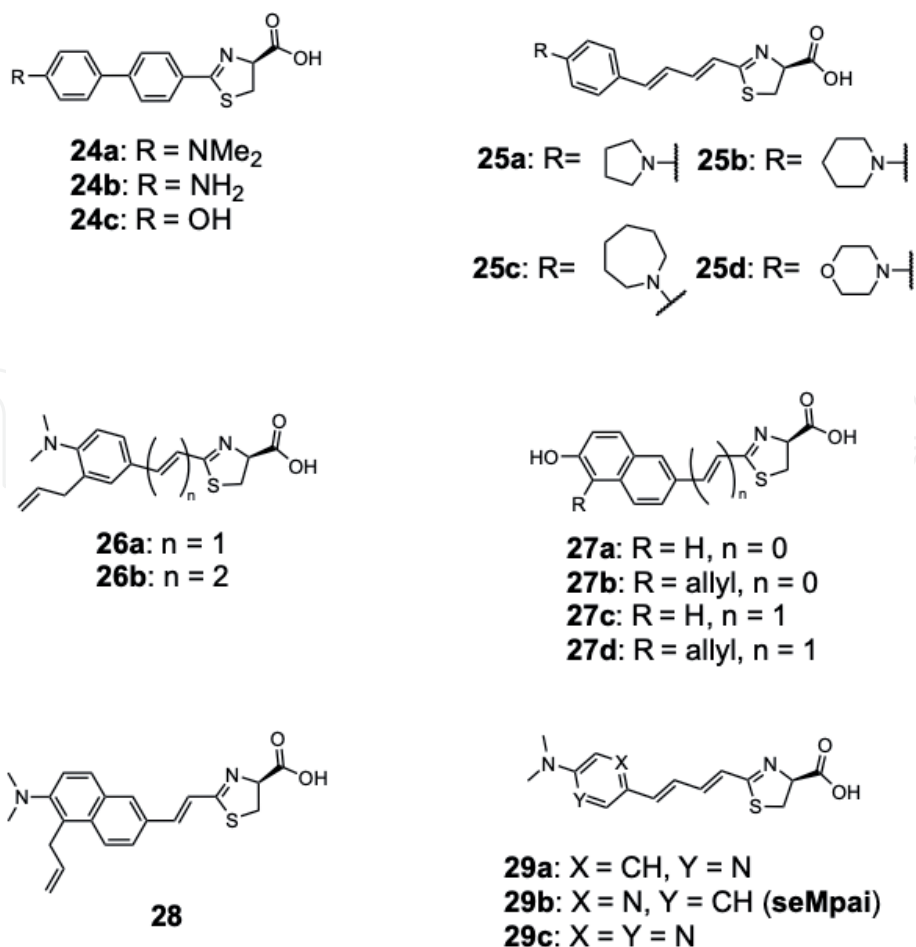


**Figure 7.**  
Structures of NIR luciferin analogs 24–29.

reaction, condensation and cyclization to obtain the final compounds **25a–d** (**Figure 8B**). Despite containing an electron-donating amino group, **25a–d** produced luminescence at almost the same wavelengths (656–667 nm) as **8e** (668 nm). However, the luminescence intensity of **25a** was approximately four times stronger than that of **8e**. The fluorescence quantum yields of **8e** and these cyclic amino analogs **25a–d** were almost identical, suggesting that the luminescence intensity largely depends on the reactivity with luciferase.

The luminescent wavelength can be lengthened not only by extending the  $\pi$ -conjugations and introducing an electron donate substituent, but also by introducing an allyl group. Kitada *et al.* synthesized allyl analogs **26a–b** (**Figure 7**) by introducing allyl groups into **8c**, **8e** and naphthol analogs **27a–d** (**Figure 7**). The analogs were introduced by two routes: Pd-catalyzed Stille coupling (**Figure 8C**) and Claisen rearrangement (**Figure 8D**) [39]. Although these analogs delivered very low luminescence intensities, their wavelength shift was long (approximately 15–35 nm). As the allyl group itself does not affect the  $\pi$ -conjugations of the substrate structure, it was considered that induce fitting was occurred at the luciferase active site and stabilized the substrate metabolite to lower energy state conformation. To develop a long-wavelength, Kitada *et al.* synthesized NIR analog (**28** in **Figure 7**) by introduced both an electron-donating NMe<sub>2</sub> and an allyl group. When reacted with Fluc, **28** produced NIR light at a sufficiently long-wavelength (705 nm), but the luminescence intensity was only 1.3% of that of **8e**. Although the allyl group extends the luminescent wavelength, it greatly reduces the luminescence intensity, which is a major disadvantage.

The aromatic ring site has also been targeted in the development of potential NIR emitters. Saito *et al.* synthesized three analogs **29a–c** (**Figure 7**) in which the

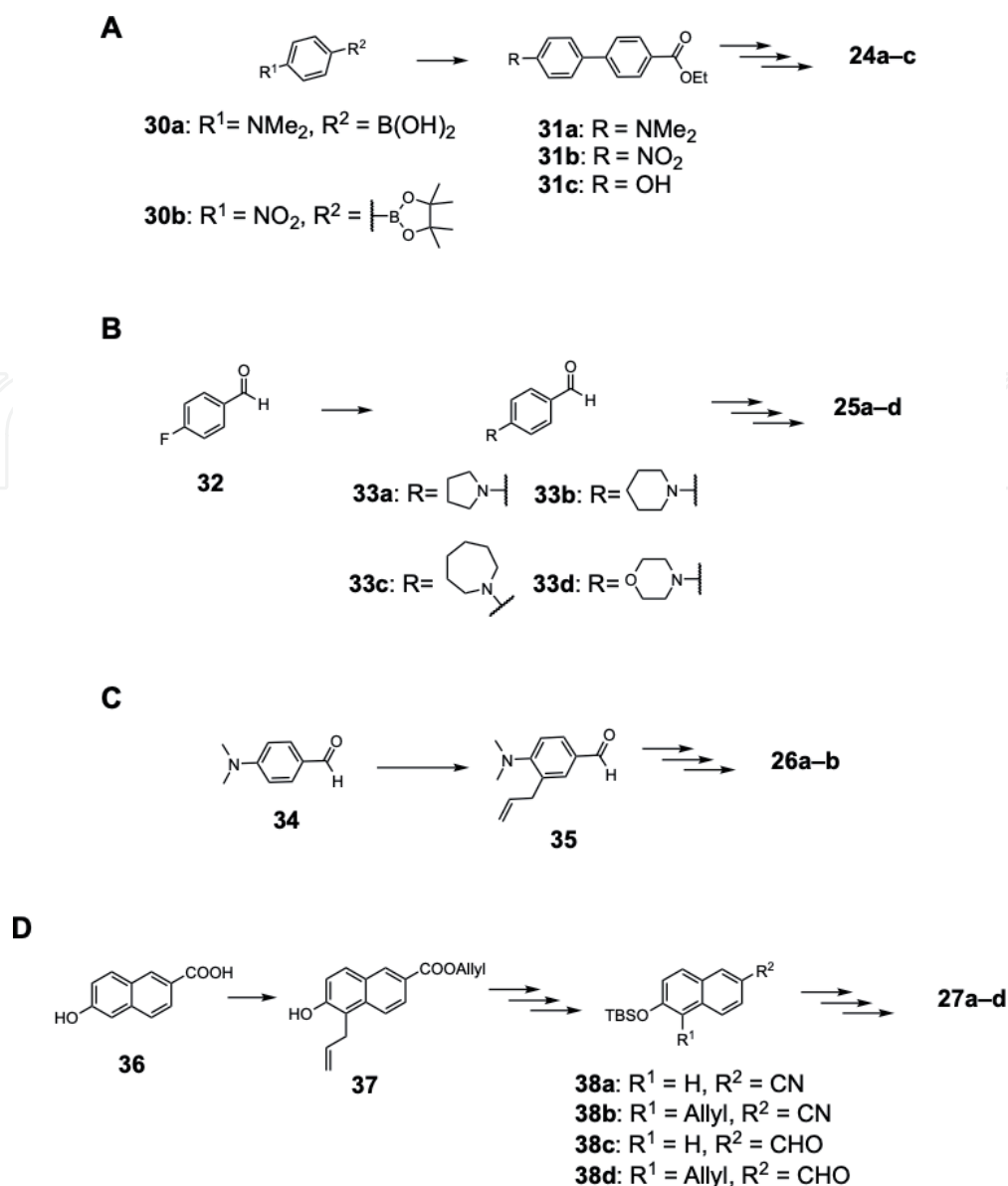


**Figure 8.**  
 Synthetic routes of NIR luciferin analogs 24a–c (A), 25a–d (B), 26a–b (C) and 27a–d (D).

aromatic ring of **8e** was replaced with an *N*-heteroaromatic ring [40]. Interestingly, the luminescence wavelengths of three analogs depended on the positions and numbers of their N atoms; **29a** produced red light at 645 nm, seMpai (**29b**) produced NIR light at 675 nm, and **29c** produced orange light at 625 nm. This result highlights the importance of interactions between the luciferase active site and the N atoms of the heterocycle. Although the luminescence wavelength of all three analogs were shorter than 700 nm, the wavelength was changed with a single atom, suggesting that interaction with the luciferase active site is an important part of molecular design.

### 3. Solubility enhancement of TokeOni and seMpai (**29b**) for sensitive *in vivo* imaging

As mentioned in the previous section, our research group has developed multicolor luciferin analogs for *in vivo* imaging. The luminescence activities of AkaLumine (**8e**) and seMpai (**29b**) are potentially suitable for BLI. Therefore, the usefulness of these analogs as reagents for *in vivo* BLI was evaluated in further animal experiments.

### 3.1 Development of AkaBLI (TokeOni and AkaLuc)

Prior to administering the reagent into the animal models, we increased the aqueous solubility of **8e** (which is inherently low) and developed an HCl salt of **8e**, AkaLumine-HCl (Tokeoni) [21]. In ultrapure water, the solubility of Tokeoni was 40 mM, approximately 20 times higher than that of **8e** (2 mM). Therefore, Tokeoni enable to administered to experimental animals with a smaller solution volume and higher concentration than **8e**. Tokeoni/Fluc BLI was performed with significantly higher sensitivity than LH2/Fluc and CycLuc1/Fluc in the lungs [21] and brain [41] of mice. However, as the *in vitro* luminescence intensity of Tokeoni/Fluc was lower than that of LH2/Fluc, it must be improved before imaging large animals such as marmosets.

Accordingly, Iwano *et al.* developed a mutant luciferase Akaluc specialized for Tokeoni. They developed the artificial bioluminescence system AkaBLI, which combines Tokeoni with Akaluc [42] (a mutation of 28 amino acid residues on *Ppy* luciferase). The AkaBLI luminescence intensity was approximately 10-fold higher in cells (*in vitro*), 52-fold higher in mouse lungs (*in vivo*), and 1400-fold higher in mouse brain tissue (*in vivo*) than LH2/Fluc luminescence intensity. In addition, AkaBLI detected single-cell signals from mouse lung and to quantified 1–10 cells. For large animal imaging, the authors inserted the Akaluc gene into an adeno-associated virus (AAV) vector, and introduced the recombinant AVV into the striatal neurons of marmosets. AkaBLI achieved video-rate real-time imaging of marmoset brains.

### 3.2 BLI with seMpai

seMpai (**29b**) was developed to improve two weak points in Tokeoni: neutral pH and disturbance by hepatic background signals. As Tokeoni is acidic [43], it may cause acidosis when injected; moreover, Tokeoni detects the hepatic background signals, which are not detected by LH2 [43, 44]. Due to the effect of N atom, seMpai was sufficiently soluble for administration to experimental animals and 69 mM was dissolved in phosphate buffered saline (pH 7.4) [40]. In Fluc-expressing lung cancer model mice, the sensitivities of seMpai and Tokeoni were not significantly different [40], but seMpai detected no hepatic background signals and seMpai BLI detected breast cancer micro-metastasis [43]. When repeated with Tokeoni and LH2, this experiment was unsuccessful. Although seMpai/Fluc was less sensitive than AkaBLI for single-cell imaging, its imaging sensitivity could be improved mutant luciferases such as Akaluc.

Fukuchi *et al.* monitored the expression of brain-derived neurotrophic factor (BDNF) in *Bdnf-luc* transgenic mice with LH2, Tokeoni, and seMpai [45]. Tokeoni achieved the most sensitive BLI, and seMpai and LH2 were comparable. The result probably reflects the different abilities of the compounds to penetrate the blood–brain-barrier. This result also indicates the necessary of evaluating the imaging reagent in terms of both its luminescence activity and pharmacokinetics.

Additionally, biocompatibility such as cytotoxicity of Tokeoni and seMpai has not been reported yet. No acute toxicity or adverse side effects were observed in mice when these compounds were administered at a concentration of 33 mM [40], however, preliminary experiments are recommended when using new analogs, not limited to Tokeoni and seMpai.

## 4. Conclusion

By investigating the structure–activity relationship of luciferin analogs, researchers have developed various methods for tuning the luminescence

wavelengths of these analogs. However, the intensity of the luminescence is poorly controlled. If the luminescence intensity and structure–activity relationships could be associated by a predictable law, we could synthesize new luciferin analogs with high luminescence intensity, and further develop an imaging technology with greater usefulness than conventional technologies.

For a practical imaging technology, both the luminescent substrate/enzyme activity and the pharmacokinetics are very important. Improving the various properties of the substrates and enzymes will enhance the sensitivity of bioluminescence imaging.

## Acknowledgements

We thank the members of Maki's and Aoyama's laboratory, and Kurogane Kasei Co., Ltd. for meaningful discussions and support.

## Conflict of interest

The authors declare no conflict of interest.

## Author details

Ryohei Saito-Moriya<sup>1,2,3</sup>, Rika Obata<sup>1</sup> and Shojiro A. Maki<sup>1,2\*</sup>

<sup>1</sup> Department of Engineering and Science, Graduate School of Informatics and Engineering, The University of Electro-Communications, Tokyo, Japan

<sup>2</sup> Center for Neuroscience and Biomedical Engineering, The University of Electro-Communications, Tokyo, Japan

<sup>3</sup> School of Pharmacy, Tokyo University of Pharmacy and Life Sciences, Tokyo, Japan

\*Address all correspondence to: [s-maki@uec.ac.jp](mailto:s-maki@uec.ac.jp)

## IntechOpen

© 2021 The Author(s). Licensee IntechOpen. This chapter is distributed under the terms of the Creative Commons Attribution License (<http://creativecommons.org/licenses/by/3.0>), which permits unrestricted use, distribution, and reproduction in any medium, provided the original work is properly cited. 

## References

- [1] Oba Y, Konishi K, Yano D, Shibata H, Kato D, Shirai T. Resurrecting the ancient glow of the fireflies. *Sci Adv.* 2020;6(49):eabc5705. DOI: 10.1126/sciadv.abc5705
- [2] Contag PR, Olomu IN, Stevenson DK, Contag CH. Bioluminescent indicators in living mammals. *Nat Med.* 1998;4(2):245-7. DOI: 10.1038/nm0298-245h
- [3] Kim J-B, Urban K, Cochran E, Lee S, Ang A, Rice B, et al. Non-invasive detection of a small number of bioluminescent cancer cells in vivo. *PLoS One.* 2010;5(2):e9364. DOI: 10.1371/journal.pone.0009364
- [4] Badr CE, Tannous BA. Bioluminescence imaging: progress and applications. *Trends Biotechnol.* 2011;29(12):624-33. DOI: 10.1016/j.tibtech.2011.06.010
- [5] Kaskova ZM, Tsarkova AS, Yampolsky I V. 1001 lights: luciferins, luciferases, their mechanisms of action and applications in chemical analysis, biology and medicine. *Chem Soc Rev.* 2016;45(21):6048-77. DOI: 10.1039/C6CS00296J
- [6] Love AC, Prescher JA. Seeing (and using) the light: Recent developments in bioluminescence technology. *Cell Chem Biol.* 2020;27(8):904-20. DOI: 10.1016/j.chembiol.2020.07.022
- [7] Chen L, Chen Z, Zheng S, Fan L, Zhu L, Yu J, et al. Study on mechanism of elemene reversing tumor multidrug resistance based on luminescence pharmacokinetics in tumor cells in vitro and in vivo. *RSC Adv.* 2020;10(57):34928-37. DOI: 10.1039/D0RA00184H
- [8] Yamada K, Noguchi K, Kimitsuki K, Kaimori R, Saito N, Komeno T, et al. Reevaluation of the efficacy of favipiravir against rabies virus using in vivo imaging analysis. *Antiviral Res.* 2019;172:104641. DOI: 10.1016/j.antiviral.2019.104641
- [9] Bennett J, Duan D, Engelhardt JF, Maguire AM. Real-time, noninvasive in vivo assessment of adeno-associated virus-mediated retinal transduction. *Invest Ophthalmol Vis Sci.* 1997;38(13):2857-63. PMID: 9418740
- [10] Yanagihara K, Takigahira M, Takeshita F, Komatsu T, Nishio K, Hasegawa F, et al. A photon counting technique for quantitatively evaluating progression of peritoneal tumor dissemination. *Cancer Res.* 2006;66(15):7532-9. DOI: 10.1158/0008-5472.CAN-05-3259
- [11] Nakayama J, Ito E, Fujimoto J, Watanabe S, Semba K. Comparative analysis of gene regulatory networks of highly metastatic breast cancer cells established by orthotopic transplantation and intra-circulation injection. *Int J Oncol.* 2017;50(2):497-504. DOI: 0.3892/ijo.2016.3809
- [12] Kuchimaru T, Kataoka N, Nakagawa K, Isozaki T, Miyabara H, Minegishi M, et al. A reliable murine model of bone metastasis by injecting cancer cells through caudal arteries. *Nat Commun.* 2018;9(1):2981. DOI: 10.1038/s41467-018-05366-3
- [13] Fleiss A, Sarkisyan KS. A brief review of bioluminescent systems (2019). *Curr Genet.* 2019;65(4):877-82. DOI: 10.1007/s00294-019-00951-5
- [14] Manni I, de Latouliere L, Gurtner A, Piaggio G. Transgenic animal models to visualize cancer-related cellular processes by bioluminescence imaging. *Front Pharmacol.* 2019;10(March):1-12. DOI: 10.3389/fphar.2019.00235

- [15] Kuroiwa Y, Nakayama J, Adachi C, Inoue T, Watanabe S, Semba K. Proliferative classification of intracranially injected HER2-positive breast cancer cell lines. *Cancers* (Basel). 2020;12(7):1811. DOI: 10.3390/cancers12071811
- [16] Han Y, Nakayama J, Hayashi Y, Jeong S, Futakuchi M, Ito E, et al. Establishment and characterization of highly osteolytic luminal breast cancer cell lines by intracaudal arterial injection. *Genes to Cells*. 2020;25(2):111-23. DOI: 10.1111/gtc.12743
- [17] Branchini BR, Murtiashaw MH, Magyar RA, Portier NC, Ruggiero MC, Stroh JG. Yellow-green and red firefly bioluminescence from 5,5-dimethyloxyluciferin. *J Am Chem Soc*. 2002;124(10):2112-3. DOI: 10.1021/ja017400m
- [18] Branchini BR, Southworth TL, Murtiashaw MH, Magyar RA, Gonzalez SA, Ruggiero MC, et al. An alternative mechanism of bioluminescence color determination in firefly luciferase. *Biochemistry*. 2004(23):7255-62. DOI: 10.1021/bi036175d
- [19] Hirano T, Hasumi Y, Ohtsuka K, Maki S, Niwa H, Yamaji M, et al. Spectroscopic studies of the light-color modulation mechanism of firefly (beetle) bioluminescence. *J Am Chem Soc*. 2009;131(6):2385-96. DOI: 10.1021/ja808836b
- [20] Weissleder R. A clearer vision for in vivo imaging. *Nat Biotechnol*. 2001(4):316-7. DOI: 10.1038/86684
- [21] Kuchimaru T, Iwano S, Kiyama M, Mitsumata S, Kadonosono T, Niwa H, et al. A luciferin analogue generating near-infrared bioluminescence achieves highly sensitive deep-tissue imaging. *Nat Commun*. 2016;7(1):11856. DOI: 10.1038/ncomms11856
- [22] Miller SC, Mofford DM, Adams ST. Lessons learned from luminous luciferins and latent luciferases. *ACS Chem Biol*. 2018;13(7):1734-40. DOI: 10.1021/acscchembio.7b00964
- [23] Podsiadły R, Grzelakowska A, Modrzejewska J, Siarkiewicz P, Słowiński D, Szala M, et al. Recent progress in the synthesis of firefly luciferin derivatives. *Dye Pigment*. 2019;170(February):107627. DOI: 10.1016/j.dyepig.2019.107627
- [24] Li S, Ruan Z, Zhang H, Xu H. Recent achievements of bioluminescence imaging based on firefly luciferin-luciferase system. *Eur J Med Chem*. 2021;211:113111. DOI: 10.1016/j.ejmech.2020.113111
- [25] White EH, Wörther H, Seliger HH, McElroy WD. Amino analogs of firefly luciferin and biological activity thereof. *J Am Chem Soc*. 1966;88(9):2015-9. DOI: 10.1021/ja00961a030
- [26] Sharma DK, Adams ST, Liebmann KL, Miller SC. Rapid access to a broad range of 6'-substituted firefly luciferin analogues reveals surprising emitters and inhibitors. *Org Lett*. 2017;19(21):5836-9. DOI: 10.1021/acs.orglett.7b02806
- [27] Kakiuchi M, Ito S, Kiyama M, Goto F, Matsuhashi T, Yamaji M, et al. Electronic and steric effects of cyclic amino substituents of luciferin analogues on a firefly luciferin-luciferase reaction. *Chem Lett*. 2017;46(8):1090-2. DOI: 10.1246/cl.170361
- [28] Reddy GR, Thompson WC, Miller SC. Robust light emission from cyclic alkylaminoluciferin substrates for firefly luciferase. *J Am Chem Soc*. 2010;132(39):13586-7. DOI: 10.1021/ja104525m
- [29] Evans MS, Charette JP, Adams ST, Reddy GR, Paley MA, Aronin N, et al.

A synthetic luciferin improves bioluminescence imaging in live mice. *Nat Methods*. 2014;11(4):393-5. DOI: 10.1038/nmeth.2839

[30] Wu W, Su J, Tang C, Bai H, Ma Z, Zhang T, et al. cybLuc: An effective aminoluciferin derivative for deep bioluminescence imaging. *Anal Chem*. 2017;89(9):4808-16. DOI: 10.1021/acs.analchem.6b03510

[31] Iwano S, Obata R, Miura C, Kiyama M, Hama K, Nakamura M, et al. Development of simple firefly luciferin analogs emitting blue, green, red, and near-infrared biological window light. *Tetrahedron*. 2013;69(19):3847-56. DOI: 10.1016/j.tet.2013.03.050

[32] Conley NR, Dragulescu-Andrasi A, Rao J, Moerner WE. A selenium analogue of firefly D-luciferin with red-shifted bioluminescence emission. *Angew Chemie Int Ed*. 2012;51(14):3350-3. DOI: 10.1002/anie.201105653

[33] Ioka S, Saitoh T, Iwano S, Suzuki K, Maki SA, Miyawaki A, et al. Synthesis of firefly luciferin analogues and evaluation of the luminescent properties. *Chem - A Eur J*. 2016;22(27):9330-7. DOI: 10.1002/chem.201600278

[34] Jathoul AP, Grounds H, Anderson JC, Pule MA. A dual-color far-red to near-infrared firefly luciferin analogue designed for multiparametric bioluminescence imaging. *Angew Chemie Int Ed*. 2014;53(48):13059-63. DOI: 10.1002/anie.201405955

[35] Stowe CL, Burley TA, Allan H, Vinci M, Kramer-Marek G, Ciobota DM, et al. Near-infrared dual bioluminescence imaging in mouse models of cancer using infraluciferin. *eLife*. 2019;8:1-22. DOI: 10.7554/eLife.45801

[36] Hall MP, Woodroffe CC, Wood MG, Que I, van't Root M, Ridwan Y, et al.

Click beetle luciferase mutant and near infrared naphthyl-luciferins for improved bioluminescence imaging. *Nat Commun*. 2018;9(1):132. DOI: 10.1038/s41467-017-02542-9

[37] Miura C, Kiyama M, Iwano S, Ito K, Obata R, Hirano T, et al. Synthesis and luminescence properties of biphenyl-type firefly luciferin analogs with a new, near-infrared light-emitting bioluminophore. *Tetrahedron*. 2013;69(46):9726-34. DOI: 10.1016/j.tet.2013.09.018

[38] Kiyama M, Iwano S, Otsuka S, Lu SW, Obata R, Miyawaki A, et al. Quantum yield improvement of red-light-emitting firefly luciferin analogues for in vivo bioluminescence imaging. *Tetrahedron*. 2018;74(6):652-60. DOI: 10.1016/j.tet.2017.11.051

[39] Kitada N, Saitoh T, Ikeda Y, Iwano S, Obata R, Niwa H, et al. Toward bioluminescence in the near-infrared region: Tuning the emission wavelength of firefly luciferin analogues by allyl substitution. *Tetrahedron Lett*. 2018;59(12):1087-90. DOI: 10.1016/j.tetlet.2018.01.078

[40] Saito R, Kuchimaru T, Higashi S, Lu SW, Kiyama M, Iwano S, et al. Synthesis and luminescence properties of near-infrared N-heterocyclic luciferin analogues for in vivo optical imaging. *Bull Chem Soc Jpn*. 2019;92(3):608-18. DOI: 10.1246/bcsj.20180350

[41] Fukuchi M, Izumi H, Mori H, Kiyama M, Otsuka S, Maki S, et al. Visualizing changes in brain-derived neurotrophic factor (BDNF) expression using bioluminescence imaging in living mice. *Sci Rep*. 2017;7(1):4949. DOI: 10.1038/s41598-017-05297-x

[42] Iwano S, Sugiyama M, Hama H, Watakabe A, Hasegawa N, Kuchimaru T, et al. Single-cell bioluminescence imaging of deep tissue in freely moving animals. *Science*.

2018;359(6378):935-9. DOI: 10.1126/  
science.aaq1067

[43] Nakayama J, Saito R, Hayashi Y, Kitada N, Tamaki S, Han Y, et al. High sensitivity in vivo imaging of cancer metastasis using a near-infrared luciferin analogue seMpai. *Int J Mol Sci.* 2020;21(21):7896. DOI: 10.3390/ijms21217896

[44] Su Y, Walker JR, Park Y, Smith TP, Liu LX, Hall MP, et al. Novel NanoLuc substrates enable bright two-population bioluminescence imaging in animals. *Nat Methods.* 2020;17(8):852-60. DOI: 10.1038/s41592-020-0889-6

[45] Fukuchi M, Saito R, Maki S, Hagiwara N, Nakajima Y, Mitazaki S, et al. Visualization of activity-regulated BDNF expression in the living mouse brain using non-invasive near-infrared bioluminescence imaging. *Mol Brain.* 2020;13(1):122. DOI: 10.1186/s13041-020-00665-7

# We are IntechOpen, the world's leading publisher of Open Access books Built by scientists, for scientists

6,300

Open access books available

171,000

International authors and editors

190M

Downloads

Our authors are among the

154

Countries delivered to

TOP 1%

most cited scientists

12.2%

Contributors from top 500 universities



WEB OF SCIENCE™

Selection of our books indexed in the Book Citation Index  
in Web of Science™ Core Collection (BKCI)

Interested in publishing with us?  
Contact [book.department@intechopen.com](mailto:book.department@intechopen.com)

Numbers displayed above are based on latest data collected.  
For more information visit [www.intechopen.com](http://www.intechopen.com)



# Imaging Promoter Assay of Adenylyl Cyclase A Gene in *Dictyostelium discoideum* during Fruiting Body Formation by Dual-Color Bioluminescence Microscopy

Taro Hayashi, Katsunori Ogoh and Hirobumi Suzuki

## Abstract

Cyclic adenosine monophosphate (cAMP), which is derived from adenosine triphosphate through adenylyl cyclase A (*acaA*), acts as an intracellular secondary messenger and an extracellular chemotactic substance in important biological processes. In the social amoebae *Dictyostelium discoideum*, cAMP mediates cell aggregation, development, and differentiation to spore and stalk cells during fruiting body formation. The *acaA* gene is transcribed under the control of three different alternative promoters. This study aimed to develop a promoter assay for *acaA* in *D. discoideum* using bioluminescence microscopy. Here, we inserted green- and red-emitting luciferase genes into downstream of promoter regions 1 and 3, respectively. Promoter activities were visualized by bioluminescence microscopy. We confirmed the differential expression of *acaA* under the control of promoters 1 and 3 at the different stages of *D. discoideum* development. We also demonstrated the application of dual-color bioluminescence imaging in the development of an imaging promoter assay.

**Keywords:** *Dictyostelium discoideum*, adenylyl cyclase A promoter, dual-color luciferase, bioluminescence microscopy, imaging promoter assay, fruiting body formation

## 1. Introduction

Gene expression and regulation are essential processes in cellular proliferation and differentiation and are involved in morphogenesis and embryogenesis. The social amoebae *Dictyostelium discoideum* is known to have a simple life cycle, short generation time, and small genome size. Thus, it is a model organism that is often used in research on morphogenesis, especially the formation of fruiting bodies from amoeba cell aggregation. This cell aggregation is mediated by extracellular cyclic adenosine monophosphate (cAMP) [1]. Then, cAMP is secreted from the tip of the cell mound for prestalk and prespore cell migration [2]. High concentrations of extracellular cAMP are required for prestalk and prespore cell differentiation [3, 4] and spore

formation [5]. Thus, cAMP plays an important role in *Dictyostelium discoideum* development. Its synthesis is catalyzed by adenylyl cyclases A, B, and G, which are encoded by the genes *acaA*, *acrA*, and *acgA*, respectively [6, 7].

Adenylyl cyclase A is considered a development-specific enzyme [8, 9]. Galardi-Castilla et al. [10] characterized the promoter region of the *acaA* gene in *Dictyostelium discoideum* Ax4 cells by histochemistry using a *lacZ*/X-Gal staining system,  $\beta$ -galactosidase reporter system, quantitative RT-PCR, and *in situ* hybridization. The *acaA* gene is transcribed under the control of three different alternative promoters: promoter 1 (distal region), promoter 2 (intermediate region), and promoter 3 (proximal region). Promoter 1 is active during the cell aggregation stage, and promoters 2 and 3 are active in the mound, slug, and fruiting body stages [10].

Promoter assays using histochemical techniques are quite cumbersome, as the samples have to be fixed, stained, and observed over time sequentially for each promoter. For this purpose, many samples must be prepared. On the other hand, a promoter assay using bioluminescence microscopy can be used to obtain time-lapse image data from a single experiment using one sample. This method is often used in the study of clock genes [11–13] and developmental biology [14–16]. In this chapter, we applied bioluminescence microscopy and used two luciferases in the development of an *acaA* promoter assay that can monitor *acaA* promoters 1 and 3 simultaneously during *Dictyostelium discoideum* development, and compared the result with those of histochemistry and  $\beta$ -galactosidase reporter system [10]. We also demonstrated the advantages of this promoter assay and discussed the perspectives that need further consideration.

## 2. Materials and methods

### 2.1 *Dictyostelium discoideum*

Under the National BioResource Project (NBRP), the National Institute of Advanced Industrial Science and Technology (AIST) in Japan provided the *Dictyostelium discoideum* strain Ax2 (NBRP ID: S00001). The Ax2 cells were cultured in SM/5 medium on a 1.4% agar plate at 21°C with *Klebsiella aerogenes* bacterial cells (provided by Prof. H. Kuwayama, Tsukuba University, Japan) as feed.

### 2.2 Firefly luciferase gene

Green- and red-emitting luciferases were used for the dual-color bioluminescence promoter assay. The green-emitting luciferase gene *Luci sp1* was cloned from *Luciola* sp. collected in the Belum forest, State Park, Malaysia. *Luci sp1* was modified and optimized for mammalian cell expression. Variant 1 of *Luci sp1* [17] (DNA Data Bank of Japan [DDBJ] accession no. LC632706) was used for the green vector construction. The red-emitting luciferase gene *Psa* (wild-type) was cloned from *Pristiocyclus sagulatus* collected in Tokyo, Japan. *Psa* (Wildtype) was modified and optimized for mammalian cell expression as *Psa* [18] (DDBJ accession no. LC495933). This luciferase gene was used for the red vector construction and was also deposited in the RIKEN BioResource Research Center (BRC), Tsukuba, Japan (BRC catalog no. RDB14361).

### 2.3 Construction of *adenylyl cyclase A* reporter vector

The *Dictyostelium* extrachromosomal expression vectors pDM304 (NBRP ID: G90008) and pDM358 (NBRP ID: G90009) were provided by Tsukuba

University under the NBRP and were used in the construction of two *acaA* reporter vectors involving promoters 1 and 3. The actin 15 promoter (*XhoI/BglII* restriction sites) of the pDM358 and pDM304 vectors was replaced with promoters 1 and 3 of *acaA*, respectively. The promoter regions were amplified using PCR from *Dictyostelium discoideum* Ax2 genomic DNA using the primer sets for promoter 1 (5'-GCctcgagCTTGATGAGTGGCCCAAACC-3' and 5'-GCagatctATTTTTAAAGATCCAAGAATTCG-3') and promoter 3 (5'-GCctcgagACCTCACTTCATAAATATATCTTTG-3' and 5'-GCagatctTTTTTAATAATTTTTTAATATTATTAC-3') [10]. Variant 1 of *Luci sp1* (green) and *Psa* (red) luciferase genes, including the *Dictyostelium* Kozak sequence (AAAA) before the start codon, was inserted into downstream of the promoter in the pDM358 and pDM304 vectors, respectively, via the *SpeI/HindIII* restriction sites. These vectors contained the actin 8 terminator.

## 2.4 Transformation and fruiting body formation

The Ax2 cells were co-transfected with the two constructed vectors by electroporation using a MicroPulser (Bio-Rad, California, USA) according to the protocol for *Dictyostelium*. The transformant cells were selected using hygromycin (50 mg/mL) and neomycin (10 mg/mL) in HL5 medium.

Millicell Cell Culture Insert PICM 0RG50 (Merck, Darmstadt, Germany) was placed onto a 35-mm glass bottom dish, and 1.2 mL of D buffer (saline solution for *Dictyostelium*) containing 3 mM D-luciferin potassium salt (Promega, Wisconsin, USA) was added to the basolateral side of the glass bottom dish. The transformant cells were seeded onto the inside of the cell culture insert above the membrane and cultured at room temperature (21°C), facilitating the development of the mound, slug, and fruiting body.

## 2.5 Bioluminescence microscopy

The bioluminescence images of the cells were captured using an LV200 bioluminescence microscope (Olympus, Tokyo, Japan) [19, 20] equipped with a UCPLFLN 20XPH objective lens (Olympus) and an ImagEM C9100-13 EM-CCD camera (Hamamatsu Photonics, Shizuoka, Japan). The activities of *acaA* promoters 1 and 3 were visualized using BA495-540GFP (Olympus) and 610ALP (Omega, New Jersey, USA) emission filters, respectively, at an exposure time of 30 s for 24 h at 90s intervals. In addition, bright-field images were captured at an exposure time of 200 ms using the same capture sequence as that of the bioluminescence images. The time course of luminescence intensity was analyzed using TiLIA, a time-lapse image analysis software [21].

## 2.6 Fluorescence microscopy

The autofluorescence images of the cells were captured using an IX83 inverted microscope (Olympus) equipped with a U-HGLGPS excitation light source (output level 100 with ND25 filter), a U-FGFP mirror unit, and a DP74 color CCD camera. A UCPFLN 10XPH objective lens was used for mound and slug observations, and a UCPFLN 4xPH objective lens was used for fruiting body observation. Exposure time was 500 ms for all experiments.

The irradiation power of the excitation light was measured at 480 nm using a PM100D optical power meter (Thorlabs, New Jersey, USA) with an S170C sensor probe for microscopy.

### 3. Results and discussion

Bright-field and bioluminescence images of the activities of promoters 1 and 3 are shown in **Figure 1**. According to the bright-field image, the amoeba cells began to aggregate after 10 h of seeding (**Figure 1A**) and formed the mound (**Figure 1D**), slug, and fruiting body (**Figure 1F**) after 16, 18, and 20 h, respectively. The image of the slug is not shown in **Figure 1**, since the moving slug disappeared from the field of view. In the case of **Figure 1**, the slug stage was extremely short and the fruiting body formation occurred immediately from the mound.

According to the bioluminescence image, promoter 1 activity was observed in single amoeba cells. It increased gradually (**Figure 1A–C**) and peaked at the mound

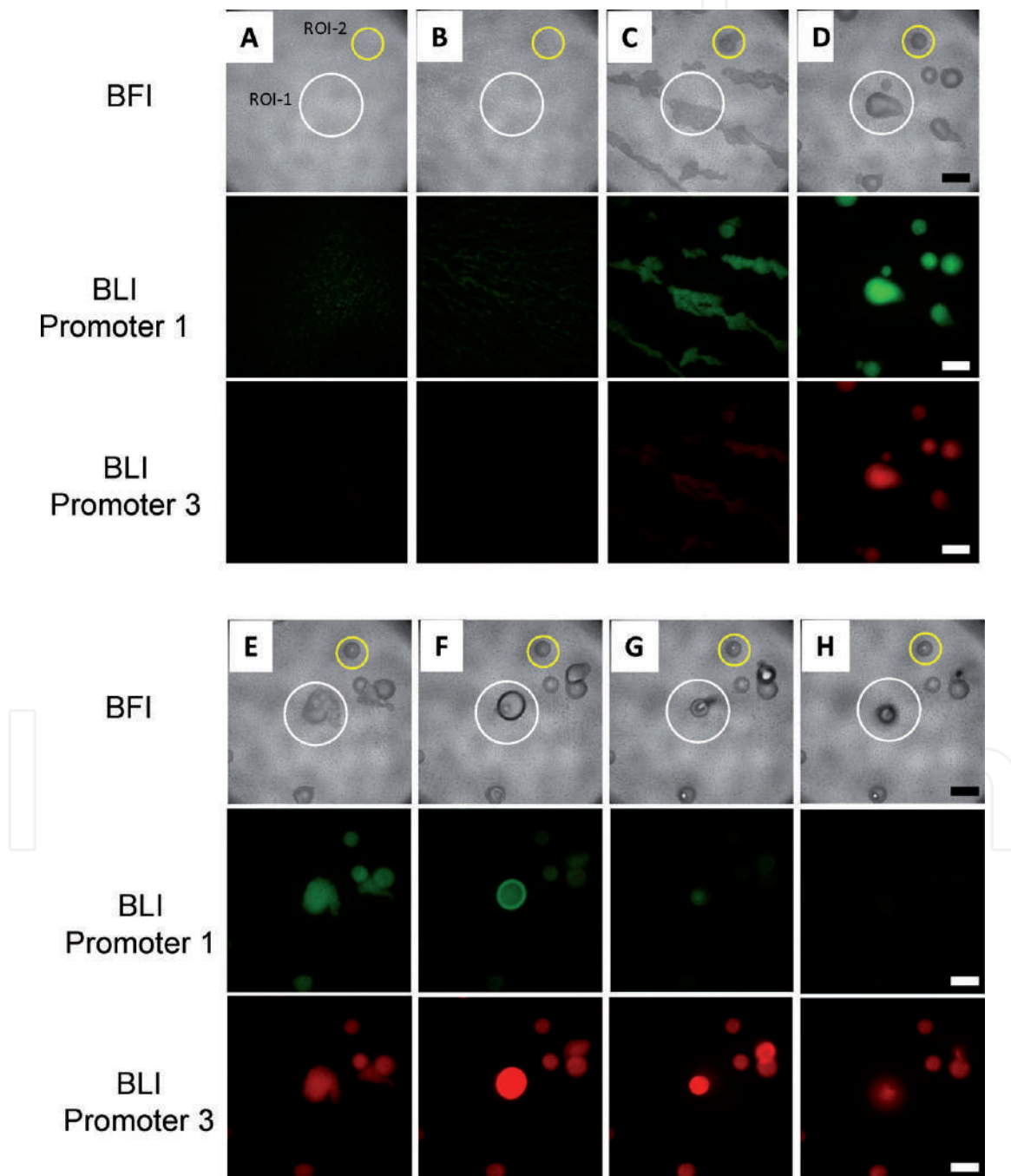


**Figure 1.** Bright-field images (BFI) and bioluminescence images (BLI) reflecting the activities of promoters 1 and 3 at 10 h (A), 12 h (B), 14 h (C), 16 h (D), 18 h (E), 20 h (F), 22 h (G), and 24 h (H) after seeding amoeba cells. Regions of interest 1 and 2 (ROI-1 and ROI-2) were assigned to cover the process from cell aggregation to fruiting body formation and are marked as circles on the BFI. Scale bar: 500  $\mu$ m.

stage after 16 h (**Figure 1D**). Then, it decreased during fruiting body formation (**Figure 1E–G**) and eventually disappeared (**Figure 1H**). On the other hand, promoter 3 activity increased during the cell aggregation stage (**Figure 1C**), peaked during the fruiting body stage (**Figure 1F**), and then decreased (**Figure 1G and H**). Thereafter, the activity of the stalk cells disappeared. Histochemical detection of promoter activity using a *lacZ*/X-Gal staining system [10] showed that promoter 1 activity was detected in the cell aggregation and early mound stages, but was not detected after the slug stage. On the other hand, promoter 3 activity was detected in the early mound, slug, and spore stages. This activity was particularly strong in the upper cup of the spores. The two methods yielded almost the same results, but

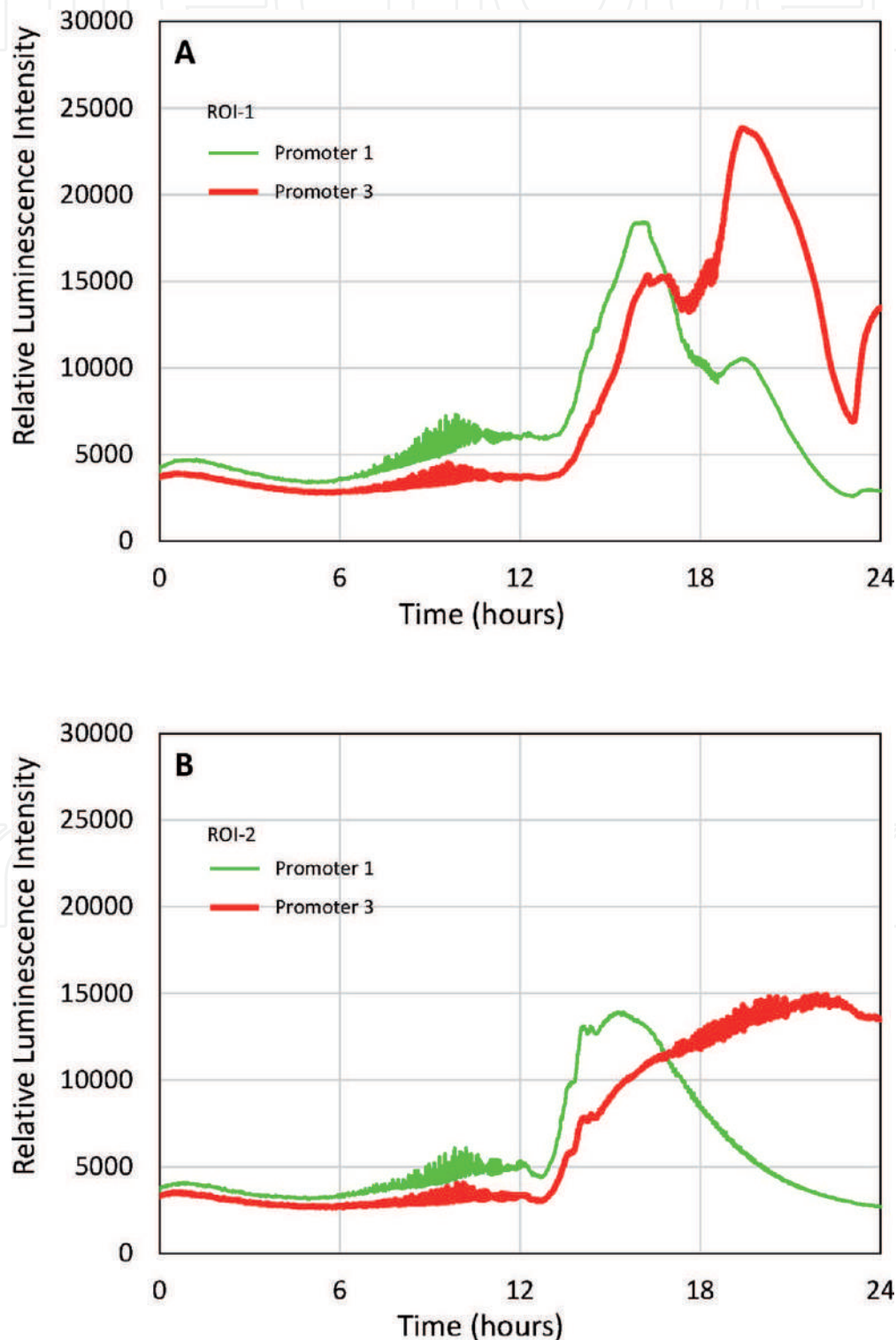


**Figure 2.**  
Time course of luminescence intensity reflecting the activities of promoters 1 and 3 in ROI-1 (A) and ROI-2 (B).

promoter 3 activity was detected earlier by bioluminescence imaging than by histochemical detection at the cell aggregation stage after 14 h (**Figure 1C**). However, the resolution of the images obtained by histochemical detection was superior to that by bioluminescence imaging.

To show the time course of the promoter activities, two regions of interest (ROI) (ROI-1 and ROI-2) were assigned to cover the process from cell aggregation to fruiting body formation, as shown in **Figure 1**. **Figure 2** shows the time course of luminescence intensity reflecting the activities of promoters 1 and 3 in ROI-1 (**Figure 2A**) and ROI-2 (**Figure 2B**) using 961 time-lapse images captured at 90s intervals for 24 h. The intensity of promoter 1 activity increased after 13 h, peaked after 16 h, decreased, and disappeared after 24 h in ROI-1 and ROI-2. On the other hand, the intensity of promoter 3 activity increased to the same timing as that of promoter 1 after 13 h, but peaked after around 20–22 h. Then, the intensity decreased gradually in ROI-2, but rapidly decreased and recovered in ROI-1. Since the measurement of the intensities involves live imaging, the discrepancy may be caused by the movement of the spores in the ROI during fruiting body formation. The measurement of the time courses of the activities of promoters 1 and 3 by bioluminescence imaging and by a  $\beta$ -galactosidase reporter system [10] showed similar results.

The results of the promoter assay using bioluminescence microscopy were the same as those of the promoter assays using histochemistry and  $\beta$ -galactosidase, confirming the convenience of this imaging promoter assay for *Dictyostelium* studies. Moreover, the imaging promoter assay enabled the spatiotemporal information of promoter activity to be obtained sequentially in a single experiment. Based on the result, detailed analysis of promoter activity can be performed efficiently by histochemical or immunofluorescence microscopy. However, several experiments are required for each measurement in histochemical and  $\beta$ -galactosidase promoter assays. Multiple promoters can also be analyzed using multicolor luciferases, but the number of promoters evaluated is limited to the number of luciferases of different colors. Moreover, there are some concerns regarding the use of multicolor luciferases in bioluminescence microscopy as follows. **Figure 3** shows the normalized

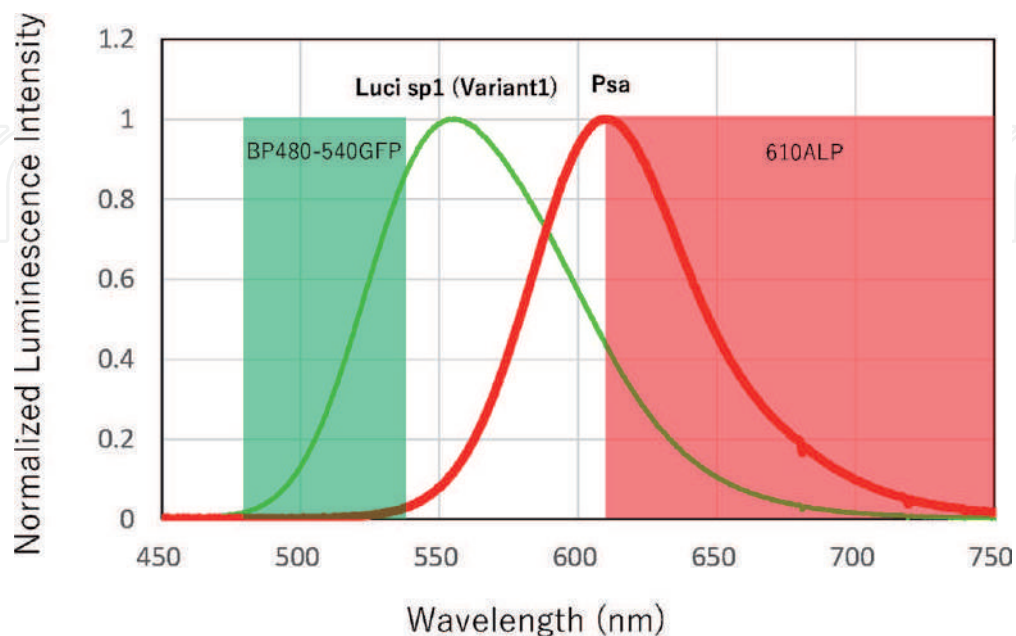


**Figure 3.** Normalized luminescence spectra of luciferases (variant 1 of *Luci sp1* and *Psa*) expressed in HeLa cells in the transparent range of the emission filters, BP480-540GFP and 610ALP.

luminescence spectra of the luciferases (variant 1 of *Luci sp1* and *Psa*) in the transparent range of the emission filter for each luciferase channel. The luciferases were expressed in HeLa cells [17, 18]. In the transparent range of the 610ALP filter, cross talk between the two spectra was observed between 610 and 700 nm. To prevent spectral cross talk, a spectral unmixing operation must be done, as is performed in fluorescence microscopy [22]. Nakajima et al. [23] demonstrated the unmixing of tri-colored bioluminescence for a luciferase promoter assay using one color to normalize the activity of two genes. In addition to the number of promoters to evaluate, we need one more color luciferase to normalize different promoter activities.

One of the advantages of bioluminescence microscopy is that it is not affected by autofluorescence background. **Figure 4** shows the bright-field and autofluorescence images of the mound, slug, and fruiting body stages of *Dictyostelium discoideum* development captured by fluorescence microscopy with a mirror unit for green fluorescent protein (GFP). Autofluorescence from the upper tip of the mound, the periphery of the slug body, and the spore and stalk of the fruiting body was observed. Therefore, the imaging conditions used GFP as a reporter require optimization of the excitation intensity, etc.

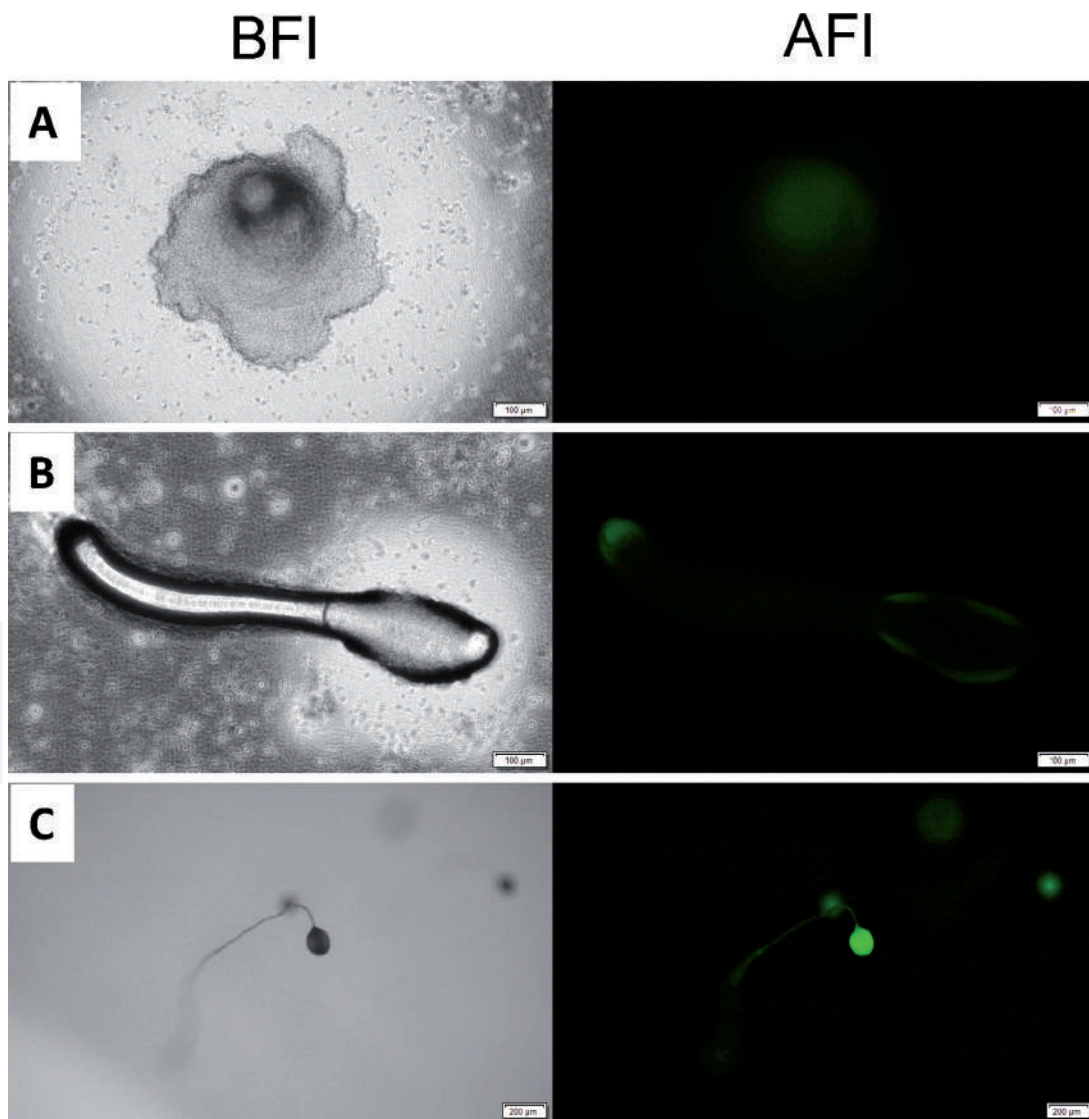


**Figure 4.** Bright-field images (BFI) and autofluorescence images (AFI) of the mound (A), slug (B), and fruiting body (C) stages of *Dictyostelium discoideum* development. Exposure time was 500 ms, and excitation light power was 0.8 mW for the mound and slug stages and 1.0 mW for the fruiting body stage. Scale bar: 100  $\mu$ m for A and B and 200  $\mu$ m for C.

## 4. Conclusion

The imaging promoter assay of the *acaA* promoters 1 and 3 by bioluminescence microscopy and the histochemical and  $\beta$ -galactosidase promoter assays yielded similar results in the evaluation *acaA* promoter activity in the different stages of *Dictyostelium discoideum* development. Moreover, we found that obtaining an overall picture of promoter activity spatiotemporally during the entire developmental process is possible with the bioluminescence imaging promoter assay. However, spectral unmixing is required to effectively normalize the different promoter activities. We also found that the imaging promoter assay is not significantly affected by autofluorescence.

## Acknowledgements

We thank Prof. H. Kuwayama (Tsukuba University, Japan) for providing the materials needed in the *Dictyostelium discoideum* experiments, offering valuable advice, and allotting time for discussion. We also thank our colleagues at Olympus Corporation for providing technical assistance during the development of the LV200 bioluminescence microscope.

This work was conducted in association with Nimura Genetic Solutions and Perak State Development Corporation for luciferase gene cloning under a contract with the Convention on Biological Diversity in Malaysia. This research did not receive grants from funding agencies in the public, commercial, or non-profit sectors.

## Conflict of interest

The authors T. Hayashi, K. Ogoh, and H. Suzuki are employees of Olympus Corporation (Tokyo, Japan).

## Author details

Taro Hayashi<sup>1\*</sup>, Katsunori Ogoh<sup>1</sup> and Hirobumi Suzuki<sup>1,2</sup>

1 Olympus Corporation, Tokyo, Japan

2 Department of Applied Chemistry, School of Advanced Engineering, Kogakuin University, Tokyo, Japan

\*Address all correspondence to: taro.hayashi@olympus.com

## IntechOpen

© 2021 The Author(s). Licensee IntechOpen. This chapter is distributed under the terms of the Creative Commons Attribution License (<http://creativecommons.org/licenses/by/3.0>), which permits unrestricted use, distribution, and reproduction in any medium, provided the original work is properly cited. 

## References

- [1] Konijn TM, van de Meene JGC, Bonner JT, Barkley DS. The acrasin activity of adenosine-3',5'-cyclic phosphate. Proceedings of the National Academy of Sciences of the United States of America. 1967;**58**:1152-1154
- [2] Dormann D, Vasiev B, Weijer CJ. The control of chemotactic cell movement during *Dictyostelium* morphogenesis. Philosophical Transactions of the Royal Society of London B. 2000;**355**:983-991
- [3] Barklis E, Lodish HF. Regulation of *Dictyostelium discoideum* mRNAs specific for prespore or prestalk cells. Cell. 1983;**32**:1139-1148
- [4] Mehdy MC, Ratner D, Firtel RA. Induction and modulation of cell-type-specific gene expression in *Dictyostelium*. Cell. 1983;**32**:763-771
- [5] Hopper NA, Anjard C, Reymond CD, Williams JG. Induction of terminal differentiation of *Dictyostelium* by cAMP-dependent protein kinase and opposing effects of intracellular and extracellular cAMP on stalk cell differentiation. Development. 1993;**119**:147-154
- [6] Saran S, Meima ME, Alvarez-Curto E, Weening KE, Rozen DE, Schaap P. cAMP signaling in *Dictyostelium*. Complexity of cAMP synthesis, degradation and detection. Journal of Muscle Research and Cell Motility. 2002;**23**:793-802
- [7] Kriebel PW, Parent CA. Adenylyl cyclase expression and regulation during the differentiation of *Dictyostelium discoideum*. IUBMB Life. 2004;**56**:541-546
- [8] Pitt GS, Milona N, Borleis J, Lin KC, Reed RR, et al. Structurally distinct and stage-specific adenylyl cyclase genes play different roles in *Dictyostelium* development. Cell. 1992;**69**:305-315
- [9] Verkerke-van Wijk I, Fukuzawa M, Devreotes PN, Schaap P. Adenylyl cyclase A expression is tip-specific in *Dictyostelium* slugs and directs Stata nuclear translocation and CudA gene expression. Developmental Biology. 2001;**234**:151-160
- [10] Galardi-Castilla M, Garciandía A, Suarez T, Sastre L. The *Dictyostelium discoideum* *acaA* gene is transcribed from alternative promoters during aggregation and multicellular development. PLoS One. 2010;**5**:e13286
- [11] Ukai H, Kobayashi TJ, Nagano M, Masumoto KH, Sujino M, Kondo T, et al. Melanopsin-dependent photoperturbation reveals desynchronization underlying the singularity of mammalian circadian clocks. Nature Cell Biology. 2007;**9**:1327-1334
- [12] Yagita K, Horie K, Koinuma S, Nakamura W, Yamanaka I, Urasaki A, et al. Development of the circadian oscillator during differentiation of mouse embryonic stem cells in vitro. Proceedings of the National Academy of Sciences of the United States of America. 2010;**107**:3846-3851
- [13] Kwon H, Enomoto T, Shimogawara M, Yasuda K, Nakajima Y, Ohmiya Y. Bioluminescence imaging of dual gene expression at the single-cell level. BioTechniques. 2010;**48**:460-462
- [14] Akiyoshi R, Kaneuch T, Aigaki T, Suzuki H. Bioluminescence imaging to track real-time armadillo promoter activity in live drosophila embryos. Analytical and Bioanalytical Chemistry. 2014;**406**:5703-5713
- [15] Morishita Y, Kuroiwa A, Suzuki T. Quantitative analysis of tissue deformation dynamics reveals three characteristic growth modes and globally aligned anisotropic tissue deformation during chick limb

development. *Development*. 2015; **142**:1672-1683

[16] Akieda Y, Ogamino S, Furuie H, Ishitani S, Akiyoshi R, Nogami J, et al. Cell competition corrects noisy Wnt morphogen gradients to achieve robust patterning in the zebrafish embryo. *Nature Communications*. 2019; **10**:4710

[17] Ogo K, Akiyoshi R, Suzuki H. Firefly luciferase. United States Patent 2014; US8722376B2

[18] Ogoh K, Akiyoshi R, Suzuki H. Cloning and mutagenetic modification of the firefly luciferase gene and its use for bioluminescence microscopy of engrailed expression during *Drosophila* metamorphosis. *Biochemistry and Biophysics Reports*. 2020; **23**:100771

[19] Ogoh K, Akiyoshi R, May-Maw-Thet, Sugiyama T, Dosaka S, Hatta-Ohashi Y, et al. Bioluminescence microscopy using a short focal-length imaging lens. *Journal of Microscopy*. 2014; **253**:191-197

[20] Suzuki H, May-Maw-Thet, Hatta-Ohashi Y, Akiyoshi R, Hayashi T. Bioluminescence microscopy: Design and applications. In: Thirumalai J, editor. *Luminescence—An Outlook on the Phenomena and Their Applications*. Rijeka, Croatia: Intech; 2016. pp. 333-349

[21] Konno J, Hatta-Ohashi Y, Akiyoshi R, Thancharoen A, Silalom S, Sakchoowong W, et al. TiLIA: A software package for image analysis of firefly flash patterns. *Ecology and Evolution*. 2016; **6**:3026-3031

[22] McRae TD, Oleksyn D, Miller J, Gao YR. Robust blind spectral unmixing for fluorescence microscopy using unsupervised learning. *PLoS One*. 2019; **14**:e0225410

[23] Nakajima Y, Kimura T, Sugata K, Enomoto T, Asakawa A, Kubota H, et al. Multicolor luciferase assay system: One-step monitoring of multiple gene expressions with a single substrate. *BioTechniques*. 2005; **38**:891-894